

1 **SO<sub>2</sub> degassing at Tungurahua volcano (Ecuador) between 2007 and 2013: transition from continuous to episodic**  
2 **activity**

3 **Hidalgo Silvana<sup>1,\*</sup>, Battaglia Jean<sup>2</sup>, Arellano Santiago<sup>3</sup>, Steele Alexander<sup>1</sup>, Bernard Benjamin<sup>1</sup>, Bourquin Julie<sup>1</sup>, Galle**  
4 **Bo<sup>3</sup>, Arrais Santiago<sup>1</sup>, Vásconez Freddy<sup>1</sup>**

5 1 Instituto Geofísico – Escuela Politécnica Nacional, Ladrón de Guevara E11-253 y Andalucía, 6to piso ed. Ing. Civil,  
6 Quito-Ecuador

7 2 Laboratoire Magmas et Volcans, Université Blaise Pascal - CNRS - IRD, OPGC, 5, Rue Kessler, 63038, Clermont-  
8 Ferrand, France

9 3 Department of Earth and Space Sciences, Chalmers University of Technology, Göteborg, Sweden

10 [shidalgo@igepn.edu.ec](mailto:shidalgo@igepn.edu.ec), [J.Battaglia@opgc.univ-bpclermont.fr](mailto:J.Battaglia@opgc.univ-bpclermont.fr), [santiago.arellano@chalmers.se](mailto:santiago.arellano@chalmers.se),  
11 [astele@igepn.edu.ec](mailto:astele@igepn.edu.ec), [bbernard@igepn.edu.ec](mailto:bbernard@igepn.edu.ec), [gingerchip@yahoo.com](mailto:gingerchip@yahoo.com), [bo.galle@chalmers.se](mailto:bo.galle@chalmers.se),  
12 [sarraais@igepn.edu.ec](mailto:sarraais@igepn.edu.ec), [fvasconez@igepn.edu.ec](mailto:fvasconez@igepn.edu.ec)

13 \* Corresponding author

14 Abstract

15 We present continuous SO<sub>2</sub> measurements performed at Tungurahua volcano with a permanent network of 4 scanning  
16 DOAS instruments between 2007 and 2013. The volcano has been erupting since September 1999, but on the contrary to the  
17 first years of eruption when the activity was quasi-continuous, the activity transitioned in late 2008 towards the occurrence  
18 of distinct eruptive phases separated by periods of quiescence. During our study period we distinguish 11 phases lasting  
19 from 17 to 527 days separated by quiescence periods of 26 to 184 days. We propose a new routine to quantify the SO<sub>2</sub>  
20 emissions when data from a dense DOAS monitoring network are available. This routine consists in summing all the highest  
21 validated SO<sub>2</sub> measurements among all stations during the 10 hours of daily working-time to obtain a *daily observed SO<sub>2</sub>*  
22 *mass*. Since measurement time is constant at Tungurahua the “observed” amounts can be expressed in tons per 10 hours and  
23 can easily be converted to a daily average flux or mass per day. Our results provide time series having an improved  
24 correlation on a long time scale with the eruptive phases and with quiescence periods. A total of 1.25 Mt (1.25 x 10<sup>9</sup> kg) of  
25 SO<sub>2</sub> has been released by Tungurahua during the study period, with 95% of these emissions occurring during phases of  
26 activity and only 5% during quiescence. This shows a contrast with previous volcanic behaviour when passive degassing  
27 dominated the total SO<sub>2</sub> emissions. SO<sub>2</sub> average daily mass emission rates are of 73 ± 56 t/d during quiescent periods, 735 ±  
28 969 t/d during long-lasting phases and 1424 ± 1224 t/d during short-lasting phases. Degassing during the different eruptive  
29 phases displays variable patterns. However, two contrasting behaviours can be distinguished for the onset of eruptive  
30 phases with both sudden and progressive onsets being observed. The first is characterised by violent opening of the conduit  
31 by high energy Vulcanian explosions; and the second by a progressive, *in crescendo*, development of the activity. The first  
32 case is becoming more frequent at Tungurahua making the volcano more dangerous and less predictable.

33

34 1. INTRODUCTION

35 1.1 Gas measurements on volcanoes

36 Surveillance of the composition and emission rate of gases from volcanoes is very important for understanding volcanic  
37 activity, especially in conditions where degassing processes have a dominant control on eruption style (Sparks et al. 1997,  
38 Oppenheimer 2003). Volcanoes emit different gaseous species such as H<sub>2</sub>O, CO<sub>2</sub>, SO<sub>2</sub>, HCl, HF, H<sub>2</sub>, S<sub>2</sub>, H<sub>2</sub>S, CO, and SiF<sub>4</sub>  
39 (Symonds et al., 1994) to the atmosphere during or between eruptions, through erupting vents, fumaroles or diffused  
40 through soil.

41 In order to obtain the concentrations of the different volcanic species, fumaroles can be sampled and collected in different  
42 condensing systems for subsequent laboratory analysis, or measured *in situ* using portable electrochemical devices. This  
43 approach allows a detailed geochemical and isotopic characterisation of the gas sample, giving strong constraints on the  
44 subsurface temperature of the volcanic-hydrothermal systems and the gas source (Allard et al. 1991, Ohba et al. 2008,  
45 Rouwet et al. 2009, Vaselli et al. 2010). Nevertheless, given the high risk implied by direct sampling, routine sampling and  
46 analysis is hard to sustain in a continuous way (Symonds et al. 1994). Besides, only peripheral emissions can usually be  
47 sampled, which may show an important degree of atmospheric dilution, thus not actually representing the conditions of the  
48 magmatic system (McGonigle and Oppenheimer 2003).

49 Remote sensing techniques such as COSPEC (Millán 1980, Stoiber et al. 1983) and DOAS-based instruments (Galle et al.  
50 2003, Edmonds et al. 2003) have been useful in measuring SO<sub>2</sub> fluxes in active (explosive), or passive (quiescent)-  
51 degassing volcanoes. The major advantage of these instruments with respect to direct sampling lies in the possibility of  
52 making long-term, integrated and frequent measurements of SO<sub>2</sub> (and other species in the case of DOAS), providing  
53 temporal series that could be correlated to seismic or ground deformation data (Nicholson et al. 2013, Conde et al. 2013,  
54 Zuccarello et al. 2013). For instance, the SO<sub>2</sub> flux data obtained with COSPEC at Etna, Pinatubo, Mount St. Helens, as well  
55 as in other erupting volcanoes, were useful tools to forecast eruptive activity (Malinconico et al. 1979, Daag et al. 1994,  
56 Casadevall et al. 1983).

57 Since the early 2000s the DOAS portable or automated systems have gradually replaced the COSPEC. The miniature UV-  
58 DOAS systems offer a series of advantages with respect to COSPEC, given their low cost and reduced size and weight  
59 (Galle et al. 2003). The mobile equipments are therefore affordable for observatories and easily transported in order to make  
60 traverses under the volcanic plume to quantify the emission flux. Moreover, the automatic scanning DOAS stations are quite  
61 resistant to very exigent weather conditions, allowing the installation of permanent instruments in the field for continuous  
62 SO<sub>2</sub> flux measurement (Edmonds et al. 2003, Arellano et al. 2008, Burton et al. 2009, Salerno et al. 2009, Conde et al.  
63 2013). As a consequence, there has been a widespread adoption of this technique by volcanological observatories, largely as  
64 part of the NOVAC network for volcanic plumes monitoring (Galle et al. 2010).

65 Continuous gas emissions datasets allow more detailed studies of degassing processes, revealing different SO<sub>2</sub> emission  
66 patterns associated with diverse eruptive dynamics and conduit processes. For instance, Burton et al. (2009) support their  
67 model of magma circulation at Stromboli during the 2007 eruption using the pattern of almost continuous SO<sub>2</sub>  
68 measurements obtained from the FLAME network. Besides, the volume of degassed magma can be estimated by measuring  
69 the original content of sulphur (S) in magmatic inclusions and in the degassed melt (Self et al. 2004, Spilliaert et al. 2006,  
70 Shinohara 2008, Métrich et al. 2010). Combining the volatile content in inclusions with good quality estimates of the  
71 released sulphur it is possible to obtain a better constraint of the amount of the so-called excess degassing in arc volcanoes  
72 (Shinohara 2008).

73 Volcanic degassing occurs under explosive or passive emission styles and it is also common to distinguish between  
74 continuously and sporadically degassing volcanoes (Shinohara 2008). Explosive degassing has the potential to produce  
75 columns reaching up to stratospheric altitudes. Passive degassing on the contrary can be produced without any magma  
76 extrusion. This degassing modality is also known as quiescent or non-eruptive. Passive degassing might last for long periods  
77 of time yielding important amounts of gas comparable to or larger than emissions from large explosive eruptions (Shinohara  
78 2008).

79 Andres and Kasgnoc (1998) published an inventory of volcanic sulphur emissions (up to 1997), including 49 continuously  
80 degassing volcanoes which exhibit persistent Hawaiian, Strombolian or Vulcanian activity, and 25 sporadically emitting  
81 volcanoes, which show more explosive but short-term eruptions (e.g. El Chichón, Pinatubo, Rabaul, Kilauea, Augustine,  
82 etc.). Comparing the amount of SO<sub>2</sub> emitted by both types of volcanoes on an annual basis, sporadically emitting volcanoes  
83 account for less than 1% of the total estimate of SO<sub>2</sub> emissions. This highlights the overwhelming importance of  
84 continuously degassing volcanoes.

### 85 *1.2 Geological setting and eruptive activity of Tungurahua since 1999*

86 Tungurahua volcano is located in central Ecuador, 120 km south of Quito. It is a 5023 m-high andesitic stratovolcano with a  
87 basal diameter of 16 km and a maximum relief of 3200 m. Tungurahua is built over the basement units of the Cordillera  
88 Real. Hall et al. (1999) distinguish three different edifices, Tungurahua I, II, and III, the latter being the present volcano.  
89 The two former edifices suffered giant landslides associated with large debris avalanche deposits found in the Chambo and  
90 Patate valleys. The activity of Tungurahua III began with the Las Juntas lava flow at about 2300 years BP (Hall et al. 1999).  
91 Since 1300 AD moderate to large eruptions producing pyroclastic flows and tephra fallouts have occurred every century, in  
92 1533, 1640, 1773, 1886, and 1918 (Le Pennec et al. 2008).

93 The present eruption of Tungurahua began in September 1999 and persists until the time of writing. Until May 2006 the  
94 activity was characterized mainly by gas and ash emissions of low to moderate intensity and discrete Strombolian and  
95 Vulcanian explosions. Six quiescence periods were observed between 1999 and 2004, two of them very short, lasting 8 and  
96 9 days; and four of intermediate duration lasting 94, 54, 58 and 46 days. A long quiescence of 353 days was observed in  
97 2005 (Figure 2a). During the whole period intense episodes of ash emission affected the local population (e.g., late 1999,  
98 August 2001) (Le Pennec et al. 2012). In May 2006 a sustained increase in activity lead to two pyroclastic-flows forming  
99 eruptions: a VEI-2 in July 2006 and a VEI-3 in August 2006 (Arellano et al. 2008; Samaniego et al. 2011; Eychenne et al.  
100 2012). These eruptive paroxysms resulted from the relatively rapid arrival of voluminous, gas rich magma from depth to an  
101 already open-vent erupting volcano according to Samaniego et al. (2011) and Eychenne et al. (2012). A detailed description  
102 of the pyroclastic flow deposits and the eruptive sequence of the 16-18 August eruption can be found in Douillet et al.  
103 (2013a, 2013b) and Hall et al. (2013). The petrological study of the juvenile material of this eruption allowed to constraint a  
104 depth of 8 to 10 km below the summit for a magmatic reservoir below Tungurahua (Samaniego et al. 2011).

105 Since 2007 we can roughly distinguish four eruptive periods based on the duration of eruptive phases (Figure 2b). (1) From  
106 February 2007 until August 2008 the volcano produced a long-lasting eruptive phase (527 days), (2) Between December  
107 2008 and May 2011, six eruptive phases of intermediate duration (37 to 98 days) took place separated by 26 to 179 days of  
108 quiescence. (3) From November 2011 until September 2012 almost continuous activity was present being more intense at  
109 the beginning and at the end of this period. (4) Short-lasting eruptive phases with durations between 17 and 27 days,

110 separated by quiescence periods between 41 and 58 days, occurred since December 2012 until August 2013. During these  
111 periods the eruptive activity included episodic explosions of Strombolian and Vulcanian styles, sub-continuous ash  
112 emissions and lava fountaining. Pyroclastic flows were also produced during some of these phases either fed by sustained  
113 lava fountains or triggered by Vulcanian events. Small to moderate ash emissions were common throughout periods of  
114 activity (Bernard et al. 2013).

115 The first SO<sub>2</sub> flux measurements at Tungurahua were done using a COSPEC. Fluxes of about 2500 t/d were observed at the  
116 beginning of the present eruptive period in August 1999, and up to 11000 t/d were measured in October 1999, presumably  
117 when magma reached the surface. The first DOAS automatic scanning network installed at Tungurahua was very similar to  
118 the one installed at Montserrat (Edmonds et al. 2003) and operated from June 2004 to November 2007. This network  
119 allowed us to record the first set of continuous SO<sub>2</sub> measurements at the volcano and to make correlations between SO<sub>2</sub>  
120 fluxes and seismicity (Arellano et al. 2008).

121 Up to 2007 Tungurahua can be classified as a continuously degassing volcano despite the low fluxes recorded during  
122 quiescent periods. Arellano et al. (2008) distinguish between passive and explosive degassing patterns during 1999-2006,  
123 based on a threshold of explosiveness measured by seismic sensors. The inferred phases of explosive degassing were  
124 manifested superficially by lava fountains, Strombolian episodes, Vulcanian explosions and regional ash fallout. On the  
125 contrary, passive degassing corresponded to low activity phases with weaker gas emissions and occasionally a limited  
126 amount of ash. The mean SO<sub>2</sub> emission rates measured during 1999-2006 were about  $2400 \pm 4600$  ( $\pm 1\sigma$ ) t/d for explosive  
127 degassing and  $1400 \pm 1700$  ( $\pm 1\sigma$ ) t/d for passive degassing (Arellano et al. 2008).

128 In this paper we describe and analyse the degassing patterns registered by the gas flux sensors at Tungurahua since February  
129 2007. In particular we intend to study the change in eruptive style from quasi-continuous degassing, as it was observed  
130 during the first years of the eruption, to an alternation of periods of quiescence and low-to-high intensity explosive activity  
131 phases.

## 132 2. DOAS MEASUREMENTS AND MONITORING NETWORK

### 133 2.1 DOAS technique

134 The principle to quantify volcanic gas fluxes using scanning instruments is a straightforward application of mass  
135 conservation in a volume enclosing the volcanic source. The scanning surfaces of the instruments surrounding a volcano  
136 define a volume (bounded from below by the ground and considered limited from above by the highest measurable altitude  
137 of the plumes) within which the main source of emission is the volcano. Thus, if no other important sources (e.g.,  
138 anthropogenic sources, chemical reactions) are present and if loss mechanisms (e.g., ground deposition, chemical reactions,  
139 adsorption in tephra, solution in aerosols, atmospheric dilution) can be neglected, the source strength is equivalent to the  
140 integral of the normal component of the flux density across the scanned surfaces. This integral is obtained by summing the  
141 column densities of the gas of interest along the transversal direction of transport, which are obtained by the spectroscopic  
142 method known as DOAS (Platt and Stutz, 2008), and multiplying the result by the normal component of the transport speed,  
143 assumed to be equal to the wind speed at a representative altitude of the plume.

### 144 2.2 DOAS Network at Tungurahua

145 The DOAS monitoring network at Tungurahua is composed of 4 NOVAC version I instruments (Galle et al. 2010). The  
146 stations are located at Huayrapata, 9.1 km Northwest of the volcano summit, Pillate, 8 km West, Bayushig, 11.9 km  
147 Southwest and Runtún, 5 km North (Figure 1). Huayrapata and Bayushig were installed on March 17 and 30, 2007, on the  
148 same sites as the previous stations described by Arellano et al. (2008). Pillate was installed on November 15, 2007, on a site  
149 located in the direction of the prevailing winds. Runtún was installed on February 23, 2011, to cover the occasional winds  
150 blowing to the North from November to December. These sites give us an almost complete coverage for plumes heading  
151 towards S to NE (clockwise), leaving only a coverage gap for infrequent plumes transported to the E-SE. Each station works  
152 during daylight from 07:00 to 17:00 (local time), all year long since sunrise and sunset times are almost constant at the  
153 latitude of the volcano. Each individual scan takes between 3 and 14 minutes, depending on the light intensity, yielding for  
154 each instrument a total of 50 to 140 scans per day. The collected data are transmitted in real time by radio link to the  
155 Tungurahua Volcano Observatory (Figure 1), where they are evaluated by the NOVAC software (Johansson et al. 2009) and  
156 post-processed daily by the observatory staff, to account for the best available wind information. Since the installation of the  
157 DOAS network the instruments have been operational for about 86% of the time for Bayushig, 85% for Pillate, and 78% for  
158 Huayrapata and Runtún.

### 159 *2.3 Data Processing*

160 The NOVAC software performs an automatic preliminary SO<sub>2</sub> flux estimation during acquisition using default or operator  
161 pre-set wind parameters (wind speed and wind direction) and plume height (Galle et al. 2010). For Tungurahua, we use the  
162 forecasted ECMWF data (<http://www.ecmwf.int>) as the default wind parameters with a time resolution of 6 hours and  
163 interpolated to the coordinates of the volcanic summit. For the plume height we assume that emissions are confined to the  
164 summit altitude of the volcano. In order to incorporate real wind conditions and plume height, which constitute an important  
165 source of error (Burton et al. 2009, Salerno et al. 2009, Johansson et al. 2009), data are post-processed on a daily basis. To  
166 post-process the data, we determine the wind speed, the wind direction and the plume height for the different time periods  
167 when triangulation between data from at least two stations is possible (Arellano et al. 2008). The only input required for this  
168 processing is the wind speed, which is taken from the VAAC (Volcanic Ash Advisory Centre) when available, or from the  
169 ECMFW (analysed data). This file is imported into the NOVAC software and SO<sub>2</sub> fluxes are calculated using the wind  
170 parameters and plume height obtained by triangulation. This geometrical strategy is not always possible when SO<sub>2</sub>  
171 emissions are very low or not continuous during the day, or when clouds affect the measurement conditions at one or more  
172 of the stations. In such a case we use a standard plume height at the altitude of the volcano summit assuming the plume is  
173 drifting at the summit's altitude (5 023 m asl) and wind velocity and direction from the ECMWF (analysed data for the  
174 corresponding day) for the flux calculation.

175 After post-processing a list is generated including the time of all valid scans taken during the day and their corresponding  
176 SO<sub>2</sub> fluxes, as well as ancillary information (plume speed, direction, height, number of spectra per scan, etc.). Valid scans  
177 are those in which SO<sub>2</sub> is measured (good spectroscopic fitting, see Galle et al. 2010 for details) and plume completeness is  
178 higher than 0.5 (an empirical measure of how well the scan captures the entire plume, equal to 1 when spectra from the low  
179 scan angles do not include signatures of the volcanic gas, Johansson, 2009). For some days the program validates only few  
180 or no scans. This can be related to several factors: plume drifting in a direction not covered by the network (SE for  
181 Tungurahua), adverse weather conditions (heavy rain or dense fog), very low SO<sub>2</sub> emissions or very large amounts of ash or  
182 aerosols emitted from the volcano. The number of daily validated measurements varies, however, strongly and empirically

183 we note that this number is usually much higher during periods of activity than during quiescence. This suggests that the  
184 low values or absence of SO<sub>2</sub> during quiescence periods is the major source of scan rejection.

185 It is noteworthy that there is an important error in the gas flux measurements performed by DOAS instruments. This error is  
186 estimated to be about 26% under good measuring conditions and about 54% under fair conditions (Galle et al. 2010, Kern et  
187 al. 2009).

### 188 3. EVALUATION OF DAILY SO<sub>2</sub> EMISSIONS

189 The conventional way to process SO<sub>2</sub> flux data, while using single or a few daily COSPEC or Mobile DOAS measurements  
190 is to average the obtained fluxes and extrapolate them as a daily flux, implicitly assuming that those measurements are  
191 representative of the whole day SO<sub>2</sub> emission (i.e. daily SO<sub>2</sub> mass). This practice is specially used for monitoring purposes  
192 in order to follow the evolution of degassing and provide scenarios of eruptive activity on a daily basis. This extrapolation is  
193 somehow justified by the reduced number of measurements and by the fact that when performing COSPEC or Mobile-  
194 DOAS the operator is able to constrain the width, height and direction of the plume, reducing therefore the uncertainties in  
195 the corresponding calculated flux. However, bad weather conditions or the presence of considerable amounts of ash might  
196 prevent obtaining reliable estimates. Moreover, activity may be highly variable during a single day, displaying sporadic or  
197 continuous degassing, and even in this last case, SO<sub>2</sub> fluxes can strongly vary during the length of a same day. Automated  
198 DOAS stations have the advantage of producing a high number of daily measurements and giving insights into the temporal  
199 evolution of degassing, with the condition that the plume axis lays within a certain range of directions above the station. The  
200 use of multiple monitoring stations allows us to cover different wind directions in which the plume might be dispersed.  
201 Averaging variable amounts of measurements to obtain *extrapolated SO<sub>2</sub> daily emission* may sometimes be an  
202 oversimplified approach, especially when a dense network is present. Therefore, in order to obtain more accurate daily  
203 estimations of the SO<sub>2</sub> emission, we developed a method that takes into account all measurements taken from the 4 stations  
204 to obtain a *daily observed SO<sub>2</sub> mass*.

#### 205 3.1 Extrapolated SO<sub>2</sub> daily emissions

206 An advantage of using the NOVAC-DOAS stations is the possibility of having numerous SO<sub>2</sub> measurements per day. At the  
207 Tungurahua Volcano Observatory, the standard way to process these data is to calculate the average of all valid  
208 measurements individually for each station and then report the highest average daily value obtained. This assumes that the  
209 highest average represents the best estimate of the true real flux when the plume direction does not vary much across the  
210 day. This approach presents, however, some inconveniences. First, the instruments work only during daylight hours (10  
211 hours at Tungurahua's latitude). Consequently, when extrapolating the measured average, it is assumed that the daylight SO<sub>2</sub>  
212 emission rate is also representative of the night time period. Second, the number of valid measurements is variable  
213 depending on the factors mentioned above, especially during phases of low or no eruptive activity when instruments record  
214 only a few valid measurements (< 10) and which in some cases may reach relatively high SO<sub>2</sub> flux values (> 1000 t/d for  
215 Tungurahua). Extrapolating these few measurements may thus result in an overestimation of the actual daily SO<sub>2</sub> emission.  
216 Besides, while prevalent wind direction at Tungurahua is to the West, variations can occur during the day and accordingly  
217 higher recorded values from other stations might be ignored because only the station with the highest daily average is taken  
218 into account.

219 To examine the influence of the data selection in the calculation of extrapolated SO<sub>2</sub> daily emissions, we tested different  
220 thresholds for the plume completeness parameter: 0.5, 0.8 and 0.9 (Figure 3). Using a threshold of 0.8 slightly reduces the  
221 number of validated measurements and provides comparable SO<sub>2</sub> emissions to those obtained by using a plume  
222 completeness threshold of 0.5 (Figure 3a). On the contrary, the 0.9 threshold reduces drastically the number of valid  
223 measurements (Figure 3b). In particular, during quiescence phases the number of validated measurements is often very low  
224 or even null and therefore the extrapolated daily emissions may be significantly reduced or can be zero despite the fact that  
225 SO<sub>2</sub> has been partially observed by the instruments.

### 226 3.2 Daily Observed SO<sub>2</sub> mass

227 Alternately, in order to determine the *daily observed mass* of SO<sub>2</sub>, we developed a procedure in which we integrate the  
228 highest available flux measurements among all stations. To achieve this, for each day, we scan the available time series  
229 between 07:00 and 17:00 (local time) searching for the highest fluxes (Figure 4). However, NOVAC instruments do not  
230 provide regularly sampled time series, nor are they synchronized among the different instruments. This is because the  
231 durations of the individual scans vary depending on local light intensity. Time series may also be sparse because of  
232 invalidation of numerous complete scans where SO<sub>2</sub> was not detected. Therefore, to identify the highest fluxes we use a  
233 sliding search window with a variable duration. The window is shifted with no overlap and its length is adjusted according  
234 to the duration of the measurements. Starting at 07:00 with an arbitrary window duration of 5 minutes, we move the search  
235 window until we find flux measurements and determine the highest value among those acquired within the interval of the  
236 search window. As the highest value is selected, when two or more stations are able to see the plume, the method provides  
237 a potential correction for underestimated clouds-affected values. This highest flux is considered valid for the duration of the  
238 corresponding scan plus a constant inter-scan time, which depends on the instrument (between 0.9 and 2.5 minutes). The  
239 corresponding mass of SO<sub>2</sub> is calculated by multiplying the flux measurement by its corresponding duration of validity. The  
240 new search window size and shift are set to the last validity duration and the search is continued. Repeating this procedure  
241 for the whole period of daylight and adding the retrieved masses produces an estimate of the daily mass of SO<sub>2</sub> observed by  
242 the monitoring instruments.

243 This approach is different from those commonly used for reporting daily mean emission rates, as we do not extrapolate the  
244 available flux measurements to estimate a daily SO<sub>2</sub> mass for 24 hours but only consider the observed masses to obtain a  
245 cumulative estimate which can be expressed in tons per ten hours (t/10h). The underlying assumption is that the absence of  
246 measurements means the absence of SO<sub>2</sub> emissions from the volcano. Because this assumption is not strictly correct, our  
247 estimated masses might underestimate the real amount of SO<sub>2</sub> emitted during the 10 hours of daily measurement. However,  
248 this approach corrects for the improper extrapolation of a reduced number of data points, as often occurs during periods of  
249 low activity. In order to obtain a value over a full day (t/d or t/24h) that is comparable with the extrapolated data, we can  
250 multiply the *daily observed mass* of SO<sub>2</sub> by 2.4, given that the stations work at Tungurahua for 10 hours.

251 Comparing both resulting series leads to different SO<sub>2</sub> emission histories (Figure 5). While SO<sub>2</sub> emissions during eruptive  
252 phases are globally equivalent using both methods, degassing during quiescence episodes (passive degassing) is drastically  
253 reduced by the daily observed mass method and in consequence the total SO<sub>2</sub> emission is also lowered. During quiescent  
254 phases at Tungurahua only sporadic gas plumes or intense fumarolic activity are observed, hence degassing is a transient  
255 process. In consequence, extrapolating few flux measurements as representative of the whole day SO<sub>2</sub> emission while  
256 transient degassing behavior dominates, leads to over-estimated values. Figure 6 shows the cumulative SO<sub>2</sub> curves produced

257 by the conventional method (Extrapolated), the proposed method (Observed masses) and the 24 hours extrapolation of the  
258 proposed method (Observed masses multiplied by 2.4). The first curve reaches a high value of 2.50 Mt of SO<sub>2</sub> emitted by  
259 the volcano since 2007, while a cumulative mass of 0.52 Mt was observed, corresponding when multiplied by 2.4 to a total  
260 of 1.25 Mt of SO<sub>2</sub>. This last curve reflects well the periods of SO<sub>2</sub> emission by changes in the slope. Flat segments represent  
261 quiescence periods, light slope long periods of continuous/sub-continuous activity (periods 1 and 3) and high slopes  
262 represent shorter phases of activity (periods 2 and 4).

### 263 *3.3 Car based traverses*

264 In order to corroborate the results obtained with the permanent network, we have performed Mobile DOAS traverses,  
265 especially during periods of high activity. Our Mobile DOAS system consists of a mini-USB2000 OceanOptics  
266 spectrometer coupled to a zenith-viewing telescope by a quartz fiber. To acquire and process the spectra we used the  
267 Mobile-DOAS v.5 software by Zhang and Johansson (2009). An external GPS antenna provides precise location and time in  
268 order to calculate the integral of the flux across the section of the plume. Usually 4 to 6 traverses are done in one day  
269 through the Baños-Penipe route, to the west of the volcano (Figure 1).

270 Mobile DOAS data are processed using the same source of wind velocity as for the processing of data from the permanent  
271 stations. Wind direction is deduced directly from the traverse, and plume height is not necessary (at least not directly, since  
272 it is required to retrieve the wind speed at the altitude of the plume). Completeness of the plume is assured for traverses in  
273 most of the cases. Traverses tend to give higher columns than scanning measurements, highlighting the effect of dilution  
274 due to scattering of radiation below the plume. This effect is more pronounced for measurements taken from the scanners  
275 due to their greater distance from the source. However, globally, the fluxes obtained by Mobile DOAS coincide (within  
276 uncertainties) with those provided by the permanent stations (Figure 7). The better similarity between the traverses and the  
277 extrapolated or observed daily estimates depends on the representativeness of the traverses in reference with the overall  
278 daily degassing as well as on the stability of the degassing during the day.

279

## 280 4. TYPES OF ACTIVITY

281 We distinguish three types of activity during the 2007-2013 period: (1) Quiescence, (2) Low explosive activity and (3) High  
282 explosive activity (Figure 2). This distinction is based on the seismo-acoustic recordings and activity reports from the  
283 Tungurahua Volcano Observatory (OVT) (<http://www.igepn.edu.ec>). The seismo-acoustic records allow differentiating  
284 between periods with only Strombolian-type activity and periods when Vulcanian-type outbursts also occur. This distinction  
285 is done by quantifying the intensity of infrasound radiation emitted during explosions. Using a network of 4 infrasound  
286 sensors located between 5 and 7 km from the vent (Kumagai et al. 2010), we normalize the peak-to-peak pressure amplitude  
287 at each station to a distance of 1 km from the source and calculate the average over the 4 stations (Steele et al. 2014). We  
288 then consider Vulcanian explosions to be those whose mean acoustic excess pressure is  $\geq 100$  Pa at a distance of 1 km, as  
289 consistent with Johnson (2003). The observatory reports complete the description of surface phenomena associated with  
290 each type of activity.

### 291 *4.1 Quiescence*

292

293 *Quiescence* is characterized by a complete absence of eruptive activity or only the presence of weak fumaroles in the crater  
294 and the upper part of the cone or sporadic gas plumes. Such manifestations generally reach heights less than 200 m above  
295 the crater rim and exceptionally, up to 500 m according to OVT reports. During quiescence neither juvenile pyroclasts nor  
296 lava are emitted from the vent. Episodes of repose last from 26 to 184 days, except during the third period of activity when  
297 very short quiescence time intervals were observed (between 3 and 17 days). Seismic activity is weak during such periods  
298 with only a few long period and volcano-tectonic earthquakes.

#### 299 *4.2 Low explosive activity*

300 *Low explosive activity* (LEA) is characterized by ash and gas emissions with low-energy explosions (< 100 Pa, i.e.  
301 Strombolian) and/or small short-lasting fountains of incandescent ejecta (<500 m above the crater rim). Ash columns vary  
302 from a few hundred meters up to 3 km in height with variable ash content. Persistent ash columns can last for hours and  
303 even days, producing abundant ash fallouts. These emissions are generally accompanied by a rumbling noise yet  
304 infrequently show completely silent degassing behavior. Small rockfalls and short-runout avalanches (<1 km) of  
305 accumulated pyroclastic material have been observed on several occasions during this type of activity. The seismic signals  
306 recorded during LEA are mainly numerous small explosion quakes, long period events and tremor (occasionally harmonic).  
307 This type of activity can be considered in general as Strombolian style. No Vulcanian-type explosion is present during these  
308 episodes.

#### 309 *4.3 High explosive activity*

310 *High explosive activity* (HEA) is defined primarily by the presence of high-energy (> 100 Pa, i.e. Vulcanian) explosions that  
311 are usually accompanied by a canon shot-like sound heard in nearby areas and during the most intense outbursts, up to 30  
312 km from the vent. The eruptive columns usually vary in height between 1 and 4 km above the crater rim yet may reach 8-10  
313 km during paroxysmal events. At night time, fountains or incandescent ejecta reaching up to 1 km above the crater rim have  
314 been observed. Incandescent blocks usually remain within 2 km distance of the vent however, ballistic projectiles were  
315 observed up to 3.5 km away during a very high-energy explosion event recorded on the 14 July 2013. The ash content is  
316 generally high producing dark gray to black eruptive columns associated with intense ash falls. During some paroxysmal  
317 phases pyroclastic flows were also produced either by long-lasting fountains (6 February 2008, 4 December 2010) or  
318 triggered by high-energy Vulcanian explosions (27 March 2007, 28 May 2010, 16 December 2012, 14 July 2013). These  
319 pyroclastic flows reached distances 3 to 6.5 km from the vent. The seismic signals recorded during high explosive activity  
320 are large explosion quakes with very-long period components and N-shaped acoustic signals, long period events, harmonic  
321 and emission tremors, and volcano-tectonic earthquakes. We relate this type of eruptive activity to a Vulcanian style,  
322 alternated with more or less violent Strombolian episodes.

323

### 324 5. ERUPTIVE ACTIVITY AND SO<sub>2</sub> DEGASSING SINCE 2007

325

326 Given that the first DOAS-NOVAC stations were installed in February 2007, the record of SO<sub>2</sub> emissions for the previous  
327 period is not detailed in this paper. Between February 2007 and August 2013, eleven well-defined eruptive phases have been  
328 recognized within four main periods of activity (Figure 2). The First period consists of a long lasting activity phase (Phase I)  
329 where LEA and HEA are intercalated. A doubling of the SO<sub>2</sub> emission is seen since day 400 (Figure 8a). This increase in

330 daily mass is observed after the February 2008 paroxysm, probably indicating the arrival of a magma richer in SO<sub>2</sub>. A  
331 progressive decrease in the SO<sub>2</sub> emission is observed towards the end of the phase. No clear change in daily SO<sub>2</sub> emission is  
332 observed linked to HEA or LEA. The Second period comprises 6 activity phases lasting from 37 to 98 days (Figures 8b, c,  
333 d, e, f and g). The first phase of this period, Phase II, still displays an alternation of HEA and LEA, while the others display  
334 mostly LEA episodes at the beginning and/or at the end of the phase. In these phases globally daily SO<sub>2</sub> emission is lower  
335 for LEA episodes than for HEA, displaying a low slope in the cumulative mass curve or even producing a flat line (end of  
336 phases III, IV, V and VI). Phases V and VI begin directly by HEA, which in both cases was characterized by a sudden  
337 opening of the conduit by Vulcanian explosions leading to the formation of pyroclastic flows. For the other phases of the  
338 second period the activity increases progressively, without pyroclastic flows forming explosions. Third period is  
339 characterized by an almost continuous activity and the distinction of clear individual phases is difficult (Figure 8). HEA is  
340 observed at the beginning of the period with a rapid increase in daily SO<sub>2</sub> emission. An alternation of HEA-LEA and  
341 quiescence is observed with a cumulative SO<sub>2</sub> curve whose slope increases progressively until the end of the period where  
342 higher emission is recorded. The Fourth period comprises four activity phases lasting between 17 and 28 days (Figure 8i, j, k  
343 and l). Phases VIII, IX and XI begin directly by a HEA with Vulcanian explosions, which formed pyroclastic flows only for  
344 phases VIII and XI. Despite the HEA beginning of phase IX, the increase in the activity and degassing is progressive, as  
345 well as the decrease towards the end, forming a bell-shaped distribution for SO<sub>2</sub>. Phase X begins by only one day of LEA  
346 and a rapid increase in SO<sub>2</sub> degassing is recorded at the beginning of the phase to also gradually decrease to almost zero SO<sub>2</sub>  
347 degassing when activity fades out. Again LEA episodes display an almost flat SO<sub>2</sub> cumulative curve indicating a lower daily  
348 SO<sub>2</sub> emission for these episodes as compared to HEA. This is shown in Table 1, which summarizes the main characteristics  
349 of each phase. Indeed, for the first and third periods, when activity is more less continuous, the SO<sub>2</sub> emission associated to  
350 LEA or HEA phases is very similar. For phases of the second and fourth periods HEA episodes display higher SO<sub>2</sub> emission  
351 than LEA episodes (Table 1). Quiescence episodes are characterized by low SO<sub>2</sub> daily observed masses, despite the fact that  
352 in some cases SO<sub>2</sub> extrapolated emission (shown in turquoise in t/24h in Figure 8 might be as high as for the activity phases.  
353 Detailed description of each eruptive phase is available as Supplementary Material.

354

## 355 6. DISCUSSION

356

### 357 6.1 *Passive vs. explosive degassing*

358 Arellano et al. (2008) highlight the dominance of passive degassing at Tungurahua volcano for the eruptive period between  
359 1999 and 2006. Indeed, while the SO<sub>2</sub> emission related to explosive activity showed higher daily values, the cumulated SO<sub>2</sub>  
360 emission recorded during low activity and quiescence is higher, accounting for up to 90% of the total emission of SO<sub>2</sub>. Our  
361 analysis of the effect of the calculation method for the daily SO<sub>2</sub> emission and the differences in defining the explosive  
362 degassing could explain partially the outnumbering of passive over explosive SO<sub>2</sub> degassing during the mentioned period  
363 but certainly not all of it. Arguably, since late 2008, the general behaviour of Tungurahua volcano has changed, and  
364 quiescence episodes have become more common and longer (Figure 2). During HEA and most of the LEA episodes, the two  
365 methods of estimation, the daily extrapolated emission ( $1.60 \times 10^9$  kg) and the *daily observed masses* multiplied by 2.4 ( $1.2$   
366  $\times 10^9$  kg), produce results within the same range. In both, the periods with higher SO<sub>2</sub> emissions coincide with the periods  
367 of overall volcanic activity (Figures 5 and 8). On the contrary, when observing the results for quiescence phases, the  
368 extrapolated daily emission method displays much higher values than the observed (x 2.4) daily masses method (Figures 6

369 and 8). This is expected because the extrapolated values globally overestimate the actual SO<sub>2</sub> emission, particularly when  
370 there are few valid measurements per day, which correspond mainly to sporadic gas emissions not representative of the  
371 whole degassing behaviour during a whole day. Nevertheless, this fact has important implications for the quantification and  
372 understanding of passive degassing. The total cumulative SO<sub>2</sub> emission during quiescence phases calculated by the  
373 extrapolation method is  $5.9 \times 10^8$  kg, while using the observed masses (x 2.4) method the total SO<sub>2</sub> emission is  $7.5 \times 10^7$  kg,  
374 i.e. one order of magnitude lower. According to the observed masses multiplied by 2.4, the percentage of SO<sub>2</sub> released  
375 during quiescent phases yields only 5% of the total degassing, with a daily average mass of  $73 \pm 56$  t/d. Calculating the  
376 mass of magma involved in the eruptive period since 2007 using the different cumulative SO<sub>2</sub> emission values would lead to  
377 extremely different volumes of magma sustaining the activity. Considering the SO<sub>2</sub> emission obtained by the observed  
378 masses method, passive degassing has almost disappeared at Tungurahua since late 2008, reflecting a change in eruptive  
379 dynamics of the volcano. We propose that Tungurahua has changed from open vent activity, allowing almost continuous  
380 passive degassing, as for example Fuego in Guatemala (Lyons et al. 2010) or Popocatépetl in Mexico during fumarolic or  
381 effusive periods (Delgado-Granados et al. 2001), to a more episodic activity reflecting a partially closed system with  
382 occasional plugging of the conduit with low SO<sub>2</sub> degassing during quiescence.

383

#### 384 *6.2 Open vent vs. closed vent system: implications on the activity of Tungurahua volcano since 2008*

385 Samaniego et al. (2011) proposed that episodic injections fed magma to a modest reservoir 10 km bellow Tungurahua's  
386 crater, which in turn supplied magma to the surface between 1999 and 2005. The authors associate the intermittent enhanced  
387 explosive activity to these magma injections, but ash and gas emission activity was globally persistent (Arellano et al.,  
388 2008). During this period, variable magma supply rates explain the transition between Vulcanian and Strombolian styles  
389 (Wright et al., 2012). Bulk-rock composition of Tungurahua ashes did not change during the 1999-2005 period, indicating a  
390 chemically and probably physically homogeneous reservoir despite the different magmatic injections (Samaniego et al.,  
391 2011). Seven periods of quiescence were observed lasting between 8 to 94 days between 1999 and 2004 and a long  
392 quiescence of 353 days in 2005. Nevertheless, in all cases volcanic unrest was progressive with a clear escalating number of  
393 VT and/or LP earthquakes before equally escalating surface manifestations.

394 Since 2007, the long phases of activity (Periods 1 and 3) have been characterised by dominantly Strombolian activity.  
395 During those phases, SO<sub>2</sub> degassing has increased progressively and varied according to the intensity of the observed  
396 surface activity. This behaviour is similar to that observed until 2005 and comparable to Popocatépetl until 2000, when  
397 activity was also more-or-less continuous (Delgado-Granados et al. 2001, Arciniega-Ceballos et al. 2003). These long  
398 periods of activity display a low slope in the relation between total cumulative SO<sub>2</sub> emission and the duration of the phase  
399 (Figure 9). The daily average SO<sub>2</sub> observed mass multiplied by 2.4 during these long phases is of  $735 \pm 969$  t/d. On the  
400 contrary, the short duration phases display a higher slope in such relation (Figure 9). During these short phases (Periods 2  
401 and 4) the daily average SO<sub>2</sub> observed mass multiplied by 2.4 is of  $1424 \pm 1224$  t/d, almost twice as for long phases. These  
402 values are in the lower range of those observed in other andesitic volcanoes (Shinohara 2008). Two contrasting behaviours  
403 are observed: a) progressive increase of degassing and ash venting with or without significant explosions at the beginning of  
404 the phase, and a dominant Strombolian-like activity (Phases II, III, IV, VII, IX, X); and b) sudden or very rapid increase in  
405 the activity simultaneous to or followed by the increase in SO<sub>2</sub> emission. This last activity usually begins with small  
406 Phreatic or Vulcanian explosions followed by a more energetic Vulcanian explosion producing pyroclastic flows, one or two

407 days latter. Then, a progressive or oscillating decrease of the activity's intensity and SO<sub>2</sub> degassing is observed (Phases V,  
408 VI, IX, XI). The difference between a) and b) is the onset of the eruptive phase, which should be controlled by the  
409 conditions at the vent. In the first case, some permeability in the conduit should exist to allow a progressive gas escape that  
410 inhibits the buildup of overpressure, leading to an *in crescendo* activity pattern, typical of an open vent system. On the  
411 contrary, for the second case, sealing of the conduit seems more effective, building an important gas overpressure and  
412 producing the more energetic and violent Vulcanian explosions that ultimately open the system. This change would depend  
413 on several conditions inherent to the magma itself, like its chemical composition, viscosity, temperature and volatiles and  
414 crystal content; or related to the feeding and plumbing system (Sparks, 2003). An increase in viscosity coupled to a decrease  
415 in temperature or associated with a change in magma composition could be responsible for reducing magma permeability  
416 producing a progressive sealing of the conduit, leading ultimately to the formation of a plug and in consequence to a closed  
417 system behaviour. A detailed geochemical study of the juvenile products should be done to test this hypothesis, which is  
418 beyond the scope of this study. A lower feeding rate and/or smaller volumes of injected magma can also lead to the plugging  
419 of the system by allowing more heat loss leading to fractional crystallisation and a viscosity increase (Cashman and Blundy  
420 2000). Once the vent is open, the activity would change to more Strombolian-like style or continue with lower energy  
421 Vulcanian explosions. Short activity phases have been observed in other andesitic volcanoes, like Ruapehu and recently  
422 Popocatepetl, but the periods of quiescence in those cases seem longer (months to years) (Nakagawa et al. 1999, Arciniega-  
423 Ceballos et al. 2003). According to the relatively small size of the recent eruptions (VEI = 1; Bernard et al. 2013), it seems  
424 that the critical volume of magma required to trigger an eruption can be built up faster.

### 425 *6.3 Progressive vs. sudden onset of eruptive activity: implications on risk assessment*

426 During the phases in which a progressive increase of activity is observed and Strombolian eruptive style is dominant, ash  
427 fallout is the main hazard for local populations. In the short-term, the major impact of this phenomenon occurs on the cattle  
428 and crops growing around the volcano, which constitute the main economic activity for nearby residents. In the long-term,  
429 ash fallout might have an important impact on human health depending on the duration of exposure but also on the ash  
430 composition (Horwell and Baxter, 2006). However, the ash from Tungurahua does not contain quartz or its polymorphs,  
431 reducing the potential risk for developing respiratory chronic diseases. Exceptionally small pyroclastic flows are observed  
432 during this kind of activity; nevertheless, they are too small to reach populated areas. The progressive evolution of these  
433 eruptive phases allows the local authorities and population to implement risk assessment plans and take actions to protect  
434 the cattle and water supply.

435 On the contrary, during phases where a violent Vulcanian eruption opens the vent, the related hazards are much greater.  
436 Typically pyroclastic flows able to reach populated areas are produced during this kind of events. In May 2010, July 2013  
437 and more recently in February and April 2014 (not included in this study), pyroclastic flows killed cows and destroyed some  
438 farming zones on the flanks of the volcano. The travel time for these phenomena to reach the Baños-Penipe road is  
439 approximately 6 to 19 minutes (Hall et al. 2013). This leaves a very short time to emit an early warning and evacuate people  
440 living on the flanks of the volcano. Besides, the eruptive columns produced during these eruptions have reached up to 9 km  
441 above the summit, leading to ash plumes that can travel great distances, affecting larger areas. As an example, the ash plume  
442 from the 28 May 2010 eruption arrived at the city of Guayaquil (~ 180 km) in about 2 hours and produced ash fallout that  
443 resulted in the temporary closure of the airport. Few or no precursory signs are typically detected before this kind of  
444 activity, creating a challenge to forecast these phenomena. As these violent eruptions without precursory signs are observed

445 since 2010 at Tungurahua and more frequently during 2013-2014, new risk assessment plans should be created and  
446 implemented in the area to better protect human lives, livestock, and economic resources.

#### 447 *6.4 Relation between cumulative emission and duration of each phase*

448 The relation observed in Figure 9 between the cumulative emission of SO<sub>2</sub> and the duration of each phase of activity  
449 suggests that the magmatic system at Tungurahua follows an exponential growth of discharge. As first pointed out by Wadge  
450 (1981) for the case of basaltic systems, and expanded in more detail by e.g. Huppert and Woods (2002) or Mastin et al.  
451 (2008), who applied the model to the effusive activity of Mount St. Helens, this response occurs due to two main conditions:  
452 i) that the mass effusion rate is linearly related to the reservoir pressure; and, ii) that the magma-reservoir pressure is  
453 linearly related to the mass of magma in the reservoir (the difference between erupted and intruded magma). On the other  
454 hand, a logarithmic curve of growth is expected for systems where magma flow is controlled by rate-dependent frictional  
455 resistance, e.g., in lava dome eruptions. This interpretation should however be taken only for its heuristic value, since  
456 several uncertainties of the actual conditions at Tungurahua remain large. For this study, the most important question is to  
457 what extent the mass emission rate of SO<sub>2</sub> can be used as a proxy for the mass eruption rate? The factors controlling this  
458 dependence are: the initial sulphur content of the magma, the speciation of S between SO<sub>2</sub> and any other S-bearing species  
459 and the partition coefficient of SO<sub>2</sub> between the gas and melt phases. Finally, there is the measurement uncertainty of SO<sub>2</sub> in  
460 the plume, including all possible transformations (scrubbing, deposition, chemistry, radiative transfer effects, etc.) after  
461 emission. All these factors can change with time, making difficult to assign a one-to-one correspondence between SO<sub>2</sub> and  
462 magma discharge. But the type of relation observed in this case is just what is expected for an elastic reservoir, indicating  
463 that degassing-induced decompression of the magmatic system may well define the intensity and duration of the eruptive  
464 phases.

465 The model is proposed to account for a simple physical mechanism behind the clear observation, presented in Figure 9, that  
466 the cumulative emission of SO<sub>2</sub> for each phase of activity is not linearly scaled with the duration of its corresponding phase.  
467 Short-duration periods of activity tend to have larger intensity of emission than long-duration periods. This led us to believe  
468 that our observations support the intuitive notion that degassing is related to depressurization of the magmatic system.  
469 Moreover, the application of this simple model permits an estimate of the characteristic time of discharge for the volcano  
470  $\sim 50 \pm 34$  days compared to a mean duration of the phases of activity of  $79 \pm 29$  days and identifies a relatively small rate of  
471 magma intrusion during the discharge, which is consistent with the sporadic pattern of activity at Tungurahua. The  
472 mathematics of discharge of this system are identical to those representing the discharge of a simple capacitor-resistor  
473 electric circuit, providing a simple analogue to the magmatic system. More details are given in the Annex.

474

## 475 7. CONCLUSIONS

476 We developed a routine, which takes into account the measurements from all available DOAS stations and integrates the  
477 highest available measurements to estimate the daily masses of SO<sub>2</sub> recorded by the network during the 10 hours of daily  
478 operation. For comparison purposes with other daily extrapolated measurements these “*observed*” masses can be multiplied  
479 by 2.4, or the equivalent factor depending on the operation time of the considered network to obtain daily emission amounts  
480 of SO<sub>2</sub>. This method strongly reduces the SO<sub>2</sub> emissions during quiescent phases producing an SO<sub>2</sub> time series well  
481 correlated with the eruptive activity. During the study period, 2007-2013, Tungurahua volcano changed its behavior from a

482 more-or-less continuously degassing volcano as observed between 1999 and late 2008 to a volcano having episodic activity  
 483 without significant degassing during quiescence periods. Between February 2007 and August 2013, eleven well-defined  
 484 phases of activity occurred, lasting from 17 to 527 days, interspersed with quiescence periods lasting from 26 to 184 days.  
 485 Only between November 2011 and September 2012 (Period 3) the quiescence episodes were shorter giving an almost  
 486 continuous activity. During the phases of activity, patterns of degassing are irregular in relation with eruptive patterns,  
 487 which are also quite diverse. Nevertheless, globally high explosive activity (HEA) episodes show a higher SO<sub>2</sub> emission  
 488 than low explosive activity (LEA) episodes. Eruptive phases may start violently with strong Vulcanian explosions  
 489 accompanied by a sudden increase of SO<sub>2</sub> degassing or alternately the activity may rise progressively with a slow increase  
 490 in SO<sub>2</sub> emissions. A total of 1.2 x 10<sup>9</sup> kg of SO<sub>2</sub> has been observed during the 1266 days of both LEA and HEA activity  
 491 recorded since 2007, comprising about 95% of the total emission during the studied period. For the short-lasting phases of  
 492 activity, results show an almost linear relation between the duration of the phase and the emitted amounts of SO<sub>2</sub>. The long  
 493 duration phases show a different trend indicating a lower daily emission. These two trends can be conciliated in a general  
 494 simple model of elastic decompression of the magmatic system, with a characteristic relaxation time commensurable with  
 495 the typical duration of the eruptive phases. Our SO<sub>2</sub> time series show low to negligible SO<sub>2</sub> degassing during quiescence  
 496 periods probably due to partial or total plugging of the conduit, which in turn leads to closed system behaviour. This  
 497 interpretation is supported by the sudden and very explosive onsets observed on several occasions with few or no evident  
 498 precursory signs making it more difficult to forecast the reactivation of the volcano. This impedes the issuing of early  
 499 warnings and in consequence new risk assessment plans should be created and implemented in the area to better protect  
 500 human lives and property.

501

## 502 ACKNOWLEDGEMENTS

503 Data for this study comes from the DOAS network at Tungurahua, which is co-financed by NOVAC, SENESCYT - PIN08-  
 504 IGEPN and BID 1707-OC-EC Projects. The classification of the explosions came from the JICA seismic and infrasound  
 505 network. This research has been conducted in the context of the Laboratoire Mixte International “Séismes et Volcans dans  
 506 les Andes du Nord” of IRD. The authors greatly acknowledge all the IG staff in charge of the monitoring of Tungurahua  
 507 volcano. We would also like to thank Sonja Storm for compiling column heights from VAAC reports since 2007 and Pablo  
 508 Samaniego for insert on Figure 1. The authors kindly acknowledge the comments from Thor Hansteen, Robin Campion and  
 509 an anonymous reviewer, which greatly improve this manuscript, as well as the editorial handling by Alessandro Aiuppa.

## 510 Appendix

### 511 *Model of magma discharge of an elastic reservoir*

512 Following Wadge (1981), Huppert and Woods (2002) and Mastin et al. (2008), an exponential growth curve of magma  
 513 discharge is expected for a reservoir which overpressure  $\Delta p = p - p_0$  is linearly related to the difference between  
 514 recharged mass  $M_i$  and erupted mass  $M_e$ :  $\Delta p = C(M_i - M_e)$ . It can be shown that the constant  $C = \frac{\partial p}{\partial M}$  depends on  
 515 the reservoir and magma compressibilities, the magma density and the reservoir volume. A second assumption for an elastic  
 516 reservoir is that mass emission rate  $Q_e$  is linearly related to reservoir pressure:  $Q_e = Ap - B$ , with constants  $A$  and  $B$ .  
 517 The cumulative erupted mass can be integrated for constant mass recharge (see Appendix 2 in Mastin et al. 2008), giving:

518

$$M_e = \frac{(Ap_o - B) - Q_i}{AC} (1 - e^{-ACt}) + Q_i t \quad (A1)$$

519

520

521

522

523

524

For a discharging reservoir which has reached the necessary overpressure by accumulation of magma or other processes (crystallization-induced degassing, tectonic stress, etc.) with no recharge, the rate of mass emission can be found to be equal to:  $Q_e = (Ap_o - B)e^{-ACt}$ . The constants **A**, **B** and **C** are related to the physical variables defining the reservoir (initial overpressure, volume, compressibility), conduit (cross section, length) and magma (compressibility, density, viscosity). The details depend on the dynamic conditions of the flow and may indeed also change over time. In particular, the “characteristic time” of the discharge is  $\tau = \frac{1}{AC}$ .

525

526

527

528

529

530

531

532

533

534

535

The magma emission rate is related to the SO<sub>2</sub> gas emission rate through the relation:

536

$$M_e = M_{SO_2}^{measured} \left( \frac{M_{SO_2}^{gas}}{M_{SO_2}^{measured}} \right) \left( \frac{M_e}{M_S} \right) \left( \frac{M_S}{M_S^{SO_2}} \right) \left( \frac{M_{SO_2}^{melt + gas}}{M_{SO_2}^{gas}} \right) \left( \frac{MW_{SO_2}}{MW_S} \right) \quad (A2)$$

537

538

539

540

541

542

Where each factor on the right side represents respectively the measured gas emission rate, the ratio between measured and emitted emission rate (related to measurement uncertainty), the sulphur content of the magma, the speciation of sulphur as SO<sub>2</sub>, the partition coefficient of SO<sub>2</sub> between the melt and gas phases, and the ratio of molecular weights of S and SO<sub>2</sub>. Some of these factors are controlled by dynamic processes and may not remain constant between different phases of activity, but their time-averaged values should not vary drastically for different phases of activity. Unfortunately, we lack detailed information to determine these factors for the magma of Tungurahua in the present study

543

544

545

546

547

This simple model of discharge thus predicts the correct order of magnitude of the typical duration and recharge rate of the eruptive phases. This indicates that observing the trend of degassing gives indication of the relaxation of the magmatic overpressure leading the eruption. The above mathematical relations have the same form as the equation of discharge of a capacitor-resistor electric circuit, with the charge representing mass, voltage proportional to pressure and capacitance dependent on compressibility and other rheological properties of the magma-conduit-reservoir system.

548

549

550

Equation of the form:  $y = p1e^{-\frac{x}{p2}} + p3 + p4x$ , thus  $p2$  is the characteristic time, and  $p4$  the recharge rate (cf. A1, Figure 9).

551 REFERENCES

552 Allard P, Malorani A, Tedesco D, Cortecchi G, Turi B (1991) Isotopic study of the origin of sulphur and carbon in Solfatara  
553 fumaroles, Campi Flegrei caldera. *Journal of Volcanology and Geothermal Research* 48:139-159

554 Andres RJ, Kasgnoc AD (1998) A time-averaged inventory of subaerial volcanic sulphur emissions. *Journal of Geophysical*  
555 *Research: Atmospheres* 103(D19): 25251-25261

556 Arciniega-Ceballos A, Chouet B, Dawson P (2003) Long-period events and tremor at Popocatepetl volcano (1994-2000)  
557 and their broadband characteristics. *Bulletin of Volcanology* 65:124-135

558 Arellano SR, Hall M, Samaniego P, Le Pennec JL, Ruiz A, Molina I, Yepes H (2008) Degassing patterns of Tungurahua  
559 volcano (Ecuador) during the 1999–2006 eruptive period, inferred from remote spectroscopic measurements of SO<sub>2</sub>  
560 emissions. *Journal of Volcanology and Geothermal Research* 176(1): 151-162

561

562 Bernard B, Wade B, Hidalgo S, Bustillos J (2013) Quantification of tephra deposits from Tungurahua 2011 - 2013 eruption,  
563 Ecuador: implication on the evolution of a long-lasting eruption. IAVCEI Scientific Assembly, July 20-24, Kagoshima  
564 (Japan), session 3F, poster P8

565

566 Burton MR, Caltabiano T, Murè F, Salerno G, Randazzo D (2009) SO<sub>2</sub> flux from Stromboli during the 2007 eruption:  
567 Results from the FLAME network and traverse measurements. *Journal of Volcanology and Geothermal Research* 182(3–4):  
568 214-220

569

570 Casadevall TJ, Rose WI, Gerlach TM, Greenland LP, Ewert J, Wunderman R, Symonds RB (1983) Gas emissions and the  
571 eruption of Mount St. Helens through 1982. *Science* 221:1383-1385

572

573 Cashman K, Blundy Jon (2000) Degassing and crystallization of ascending andesite and dacite. *Philosophical Transactions*  
574 *of the Royal Society of London* 358 1770 1487-1513; doi:10.1098/rsta.2000.0600 1471-2962

575

576 Champenois, J., V. Pinel, S. Baize, L. Audin, H. Jomard, A. Hooper, A. Alvarado, and H. Yepes (2014), Large-scale inflation  
577 of Tungurahua volcano (Ecuador) revealed by Persistent Scatterers SAR interferometry, *Geophys. Res. Lett.*, 41, 5821–  
578 5828, doi:[10.1002/2014GL060956](https://doi.org/10.1002/2014GL060956).

579

580 Conde V, Bredemeyer S, Duarte E, Pacheco J, Miranda S, Galle B, Hansteen T (2013) SO<sub>2</sub> degassing from Turrialba  
581 Volcano linked to seismic signatures during the period 2008–2012. *International Journal of Earth Sciences (Geol Rundsch)*:  
582 1-16

583

584 Daag A, Tubianosa B, Newhall C, Tungol N, Javier D, Dolan M, de los Reyes PJ, Arboleda R, Martinez M, Regalado MTM  
585 (1994) Monitoring sulphur dioxide emissions at Mount Pinatubo. In: Punongbayan RS, Newhall CG (eds) *The 1991-1992*  
586 *eruptions of Mount Pinatubo, Philippines*. US Geological Survey Professional Paper

587

588 Delgado-Granados H, Cárdenas González L, Piedad Sánchez N (2001) Sulphur dioxide emissions from Popocatepetl  
589 volcano (Mexico): case study of a high-emission rate, passively degassing erupting volcano. *Journal of Volcanology and*  
590 *Geothermal Research* 108: 107-120

591

592 Douillet GA, Tsang-Hin-Sun È, Kueppers U, Letort J, Pacheco DA, Goldstein F, Aulock F, Lavallée Y, Hanson JB, Bustillos  
593 J, Robin C, Ramón P, Hall M, Dingwell D (2013a) Sedimentology and geomorphology of the deposits from the August  
594 2006 pyroclastic density currents at Tungurahua volcano, Ecuador. *Bulletin of Volcanology* 75 (11): 10.1007/s00445-013-  
595 0765-7

596

597 Douillet GA, Pacheco DA, Kueppers U, Letort J, Tsang-Hin-Sun È, Bustillos J, Hall M, Ramón P, Dingwell D (2013b)  
598 Dune bedforms produced by dilute pyroclastic density currents from the August 2006 eruption of Tungurahua volcano,  
599 Ecuador. *Bulletin of Volcanology* 75 (11): 10.1007/s00445-013-0762-x  
600  
601 Edmonds M, Herd RA, Galle B, Oppenheimer CM (2003) Automated, high time-resolution measurements of SO<sub>2</sub> flux at  
602 Soufrière Hills Volcano, Montserrat. *Bulletin of Volcanology* 65(8): 578-586  
603  
604 Eychenne J, Pennec J-L, Troncoso L, Gouhier M, Nedelec J-M (2012) Causes and consequences of bimodal grain-size  
605 distribution of tephra fall deposited during the August 2006 Tungurahua eruption (Ecuador). *Bulletin of Volcanology* 74(1):  
606 187-205  
607  
608 Galle B, Oppenheimer C, Geyer A, McGonigle AJS, Edmonds M, Horrocks L (2003) A miniaturised ultraviolet  
609 spectrometer for remote sensing of SO<sub>2</sub> fluxes: a new tool for volcano surveillance. *Journal of Volcanology and Geothermal*  
610 *Research* 119 (1-4): 241-254  
611  
612 Galle B, Johansson M, Rivera C, Zhang Y, Kihlman M, Kern C, Lehmann T, Platt U, Arellano S, Hidalgo S (2010) Network  
613 for Observation of Volcanic and Atmospheric Change (NOVAC) - A global network for volcanic gas monitoring: Network  
614 layout and instrument description. *Journal of Geophysical Research: Atmospheres* 115: D5 2156-2202  
615 <http://dx.doi.org/10.1029/2009JD011823>  
616  
617 Hall ML, Robin C, Beate B, Mothes P, Monzier M (1999) Tungurahua Volcano, Ecuador: structure, eruptive history and  
618 hazards. *Journal of Volcanology and Geothermal Research* 91(1): 1-21  
619  
620 Hall ML, Steele AL, Mothes PA, Ruiz MC (2013) Pyroclastic density currents (PDC) of the 16–17 August 2006 eruptions of  
621 Tungurahua volcano, Ecuador: Geophysical registry and characteristics. *Journal of Volcanology and Geothermal Research*  
622 265(0): 78-93  
623  
624 Horwell C, Baxter P (2006) The respiratory health hazards of volcanic ash: a review for volcanic risk mitigation. *Bulletin of*  
625 *Volcanology* 69(1):1-24  
626  
627 Huppert H, Woods A (2002) The role of volatiles in magma chamber dynamics. *Nature* 420, 493-495,  
628 [doi:10.1038/nature01211](https://doi.org/10.1038/nature01211)  
629  
630 Johansson M, Galle B, Rivera C, Zhang Y (2009) Tomographic reconstruction of gas plumes using scanning DOAS.  
631 *Bulletin of Volcanology* 71 (10): 1169-1178 <http://dx.doi.org/10.1007/s00445-009-0292-8>  
632  
633 Johansson M., Application of Passive DOAS for Studies of Megacity Air Pollution and Volcanic Gas Emissions, PhD  
634 Thesis, Chalmers University of Technology, 64 pp., 2009.  
635  
636 Johnson, J. B., 2003. Generation and propagation of infrasonic airwaves from volcanic explosions. *Journal of Volcanology*  
637 *and Geothermal Research*, **121**, 1-14.  
638  
639 Kern C, Deutschmann T, Vogel L, Wöhrbach M, Wagner T, Platt U (2010) Radiative transfer corrections for accurate  
640 spectroscopic measurements of volcanic gas emissions. *Bulletin of Volcanology* 72(2): 233-247  
641  
642 Kumagai H, Nakano M, Maeda T, Yepes H, Palacios P, Ruiz M, Arrais S, Vaca M, Molina I, Yamashima T (2010)  
643 Broadband seismic monitoring of active volcanoes using deterministic and stochastic approaches. *Journal of Geophysical*  
644 *Research: Solid Earth* 115 B8 : 2156-2202 <http://dx.doi.org/10.1029/2009JB006889>  
645

646 Le Pennec JL, Jaya D, Samaniego P, Ramón P, Moreno Yáñez S, Egred J, van der Plicht J (2008) The AD 1300–1700  
647 eruptive periods at Tungurahua volcano, Ecuador, revealed by historical narratives, stratigraphy and radiocarbon dating.  
648 Journal of Volcanology and Geothermal Research 176(1):70-81  
649

650 Le Pennec J-L, Ruiz A, Ramón P, Palacios E, Mothes P, Yepes H (2012) Impact of tephra falls on Andean communities: The  
651 influences of eruption size and weather conditions during the 1999–2001 activity of Tungurahua volcano, Ecuador, Journal  
652 of Volcanology and Geothermal Research 217–218: 91-103 ISSN 0377-0273,  
653 <http://dx.doi.org/10.1016/j.jvolgeores.2011.06.011>.  
654

655 Lyons JJ, Waite GP, Rose WI, Chigna G (2010) Patterns in open vent, Strombolian behavior at Fuego volcano, Guatemala,  
656 2005–2007. Bulletin of Volcanology 72:1-15  
657

658 Malinconico L (1979) Fluctuations in SO<sub>2</sub> emission during recent eruptions of Etna. Nature 278:43-45  
659

660 Mastin L, Roeloffs E, Beeler N, Quick J, (2008) Constraints on the size, overpressure, and volatile content of the Mount St.  
661 Helens magma system from geodetic and dome-growth measurements during the 2004-2006+ eruption: Chapter 22 in *A*  
662 *volcano rekindled: the renewed eruption of Mount St. Helens, 2004-2006*, USGS Professional Paper: 1750-22  
663

664 McGonigle A.J.S. and Oppenheimer C. (2003). Optical sensing of volcanic gas and aerosol emissions. In: Oppenheimer, C.,  
665 Pyle, D.M. and Barclay, J. (eds.) *Volcanic Degassing*, Geological Society, London. 149-168. ISBN: 978-1-86239-136-9  
666

667 Métrich N, Bertagnini A, Di Muro, A (2010) Conditions of Magma Storage, Degassing and Ascent at Stromboli: New  
668 Insights into the Volcano Plumbing System with Inferences on the Eruptive Dynamics. Journal of Petrology 51 (3): 603-626  
669 [10.1093/petrology/egg083](http://dx.doi.org/10.1093/petrology/egg083)  
670

671 Millán M (1980) Remote sensing of air pollutants: a study of some atmospheric scattering effects. Atmospheric  
672 Environment 14:1241-1253  
673

674 Morrissey, M. M., Chouet, B. A., 1997. Burst conditions of explosive volcanic eruptions recorded on microbarographs.  
675 Science, 275, 1290-1293.  
676

677 Nakagawa M, Wada K, Thordarson T, Wood CP, Gamble J (1999) Petrologic investigations of the 1995 and 1996 eruptions  
678 of Ruapehu volcano, New Zealand: formation of discrete and small magma pockets and their intermittent discharge.  
679 Bulletin of Volcanology 61 (1-2) [10.1007/s004450050259](http://dx.doi.org/10.1007/s004450050259) <http://dx.doi.org/10.1007/s004450050259>  
680

681 Nicholson EJ, Mather TA, Pyle DM, Odbert HM, Christopher T (2013) Cyclical patterns in volcanic degassing revealed by  
682 SO<sub>2</sub> flux timeseries analysis: An application to Soufrière Hills Volcano, Montserrat. Earth and Planetary Science Letters  
683 375(0): 209-221  
684

685 Ohba T, Hirabayashi J-i, Nogami K, Kusakabe M, Yoshida M (2008) Magma degassing process during the eruption of Mt.  
686 Unzen, Japan in 1991 to 1995: Modeling with the chemical composition of volcanic gas. Journal of Volcanology and  
687 Geothermal Research 175(1–2):120-132  
688

689 Oppenheimer C (2003) Volcanic Degassing. In: Rudnick RL (ed) The Crust. Treatise on Geochemistry. Elsevier-Pergamon,  
690 Oxford, pp 123-166  
691

692 Platt U, Stutz J (2008) Differential Optical Absorption Spectroscopy. Principles and Applications. Springer Berlin  
693 Heidelberg.  
694

695 Rose WI, Stoiber R, Malinconico L (1982) Eruptive gas compositions and fluxes of explosive volcanoes: budget of S and Cl  
696 emitted from Fuego volcano, Guatemala. In: Thorpe RS (ed) *Andesites: Orogenic Andesites and Related Rocks*. Wiley, New  
697 York, pp 669-676  
698

699 Rouwet, D., Bellomo, S., Brusca, L., Inguaggiato, S., Jutzeler, M., Mora, R., Mazot, A., Bernard, R., Cassidy, M., Taran, Y.,  
700 2009. Major and trace element geochemistry of El Chichón volcano-hydrothermal system (Chiapas, Mexico) in 2006–2007:  
701 implications for future geochemical monitoring. *Geofisica International*. 48 (1), 55–72.  
702

703 Salerno GG, Burton MR, Oppenheimer C, Caltabiano T, Randazzo D, Bruno N, Longo V (2009) Three-years of SO<sub>2</sub> flux  
704 measurements of Mt. Etna using an automated UV scanner array: Comparison with conventional traverses and uncertainties  
705 in flux retrieval. *Journal of Volcanology and Geothermal Research* 183(1–2):76-83  
706

707 Samaniego P, Le Pennec J-L, Robin C, Hidalgo S (2011) Petrological analysis of the pre-eruptive magmatic process prior to  
708 the 2006 explosive eruptions at Tungurahua volcano (Ecuador). *Journal of Volcanology and Geothermal Research* 199(1-  
709 2):69-84  
710

711 Self S, Gertisser R, Thordarson T, Rampino MR, Wolff JA (2004) Magma volume, volatile emissions, and stratospheric  
712 aerosols from the 1815 eruption of Tambora. *Geophysical Research Letters* 31 L20608  
713

714 Shinohara H (2008) Excess degassing from volcanoes and its role on eruptive and intrusive activity. *Reviews of Geophysics*  
715 46(4): RG4005  
716

717 Sparks RSJ, Bursik MI, Carey SN, Gilbert JS, Glaze LS, Sigurdsson H, Woods AW (1997) *Volcanic Plumes*, John Wiley &  
718 Sons Ltd, Chichester, England, 574 pp  
719

720 Sparks RSJ. Dynamics of magma degassing. *Geological Society, London, Special Publications*, 213:5-22, doi:  
721 10.1144/GSL.SP.2003.213.01.02  
722

723 Steele, A., Ruiz, M., Anzieta, A., Johnson, J. Similarities in eruption dynamics: A seismo-acoustic analysis of explosion  
724 sequences at Tungurahua volcano in May-July 2010 & December 2012. Poster presentation: European Geosciences Union  
725 (EGU) General Assembly; 2014 April 27-May 2; Vienna, Austria.  
726

727 Stoiber R, Malinconico L, Williams SN (1983) Use of the correlation spectrometer at volcanoes. In: Tazieff H, Sabroux J-C  
728 (eds) *Forecasting volcanic events*. Elsevier, Amsterdam, pp 425-444  
729

730 Spilliaert N, Métrich N, Allard P (2006) S–Cl–F degassing pattern of water-rich alkali basalt: Modelling and relationship  
731 with eruption styles on Mount Etna volcano. *Earth and Planetary Science Letters*: 248(3–4):772-786 ISSN 0012-821X,  
732 <http://dx.doi.org/10.1016/j.epsl.2006.06.031>.  
733  
734  
735

736 Symonds RB, Rose WI, Bluth GJS, Gerlach TM (1994) Volcanic-gas studies: methods, results and applications. In: Carroll  
737 MR, Holloway JR (eds) *Volatiles in Magmas*. Mineralogical Society of America, Washington, D.C. pp 1-66  
738

739 Vaselli O, Tassi F, Duarte E, Fernandez E, Poreda RJ, Huertas AD (2010) Evolution of fluid geochemistry at the Turrialba  
740 volcano (Costa Rica) from 1998 to 2008. *Bulletin of Volcanology* 72(4): 397-410  
741

742 Wadge G (1981) The variation of magma discharge during basaltic eruptions, *Journal of Volcanology and Geothermal*  
743 *Research* 11 (2-4), 139-168, DOI: 10.1016/0377-0273(81) 90020-2

744  
745 Wright H, Cashman K, Mothes P, Hall M, Ruiz A, Le Pennec J-L (2012) Estimating rates of decompression from textures of  
746 erupted ash particles produced by 1999–2006 eruptions of Tungurahua volcano, Ecuador. *Geology*, 40: 619–  
747 622,doi:10.1130/G32948.1  
748  
749 Zhang Y, Johansson M (2009) Mobile-DOAS software. Optical Remote Sensing Group Chalmers University of Technology,  
750 Sweden. Copyright © 2004–2009  
751  
752 Zuccarello L, Burton M, Saccorotti G, Bean C, Patanè D (2013) The coupling between very long period seismic events,  
753 volcanic tremor, and degassing rates at Mount Etna volcano. *Journal of Geophysical Research: Solid Earth* 118: 4910 –  
754 4921 <http://dx.doi.org/10.1002/jgrb.50363>

755

## 756 FIGURE CAPTIONS

757 **Figure 1.** SO<sub>2</sub>, seismic broadband and infrasound monitoring networks at Tungurahua Volcano. DOAS stations are shown  
758 in red with the corresponding scanning plane (flat or conic). Broadband seismic stations and infrasound detectors are show  
759 in yellow. The location of the Tungurahua Volcano Observatory is shown in green and a shaded area indicates the  
760 predominant direction of the plume. The main rivers and roads as well as populated areas are also shown.

761 **Figure 2.** Periods and phases of activity distinguished at Tungurahua volcano. a) September 1999 to August 2013. b)  
762 January 2007 to August 2013. White background indicates periods of quiescence. Yellow and orange represent low (LEA)  
763 and high (HEA) explosive activity respectively. c) Tungurahua during quiescence phases. d) and e) Typical lava fountaining  
764 (500 m above crater level) and ash venting during low explosive activity (2 km above crater level). e) Vulcanian eruption at  
765 Tungurahua, eruptive column reaches 8.8 km above crater level.

766 **Figure 3.** SO<sub>2</sub> daily extrapolated emissions for Tungurahua volcano since January 2007 until August 2013. As for Figure 2  
767 orange, yellow and white background represent HEA, LEA and quiescence. a) SO<sub>2</sub> daily emission calculated using 0.5  
768 (black bars) and 0.8 (green bars) plume completeness. Number of corresponding valid measurements during the day are in  
769 black for 0.5 and in red for 0.8. b) SO<sub>2</sub> emission calculated using 0.5 (black bars) and 0.9 (green bars) plume completeness.  
770 Number of corresponding valid measurements during the day are in black for 0.5 and in red for 0.9. Note that SO<sub>2</sub> emission  
771 for 0.5 and 0.8 plume completeness are very similar despite a slight reduction in the number of measurements, while for 0.9,  
772 the number of valid measurements is drastically reduced and for quiescence very few or no measurements are validated  
773 leading to zero emission.

774 **Figure 4.** Examples of individual SO<sub>2</sub> measurements at the 4 different stations. Coloured diamonds represent the valid  
775 individual SO<sub>2</sub> measurements at the 4 permanent DOAS stations on 30/11/2011 (left) and 12/07/2011 (right). The first day  
776 has a total of 291 valid measurements while the second has only 7. The daily average for each station is shown as a  
777 horizontal line of the same colour. A thick black line joins data points used to determine the daily observed mass of SO<sub>2</sub>. On  
778 30/11/2011 extrapolated and observed SO<sub>2</sub> x 2.4 are roughly equivalent, while on 12/07/2011 the extrapolation method  
779 clearly overestimates the total SO<sub>2</sub> emission.

780 **Figure 5.** Comparison between extrapolated (upper plot) and observed (lower plot) daily SO<sub>2</sub> mass measurements for the  
781 period between February 2007 and August 2013. Note that extrapolated SO<sub>2</sub> is expressed in tons per 24 hours while  
782 observed SO<sub>2</sub> is expressed in tons per 10 hours. Vertical scales have been scaled by a factor 2.4 to be comparable. Violet  
783 histogram shows the daily validated measurement duration (DVMD). The 4 upper lines indicate downtime periods for the

784 DOAS stations: Pillate (red), Huayrapata (maroon), Bayushig (magenta) and Runtún (green) with grey indicating periods  
785 when the stations were not yet installed.

786 **Figure 6.** Cumulative curves of SO<sub>2</sub> emission using extrapolated values, observed masses and observed masses multiplied  
787 by 2.4. Eruptive phases are marked in orange.

788 **Figure 7.** Comparison between SO<sub>2</sub> estimates obtained doing mobile-DOAS traverses and those obtained from the DOAS  
789 permanent network. Estimates from the permanent network are shown as black filled histograms for observed masses in  
790 tons per 10 hours and as empty red histograms for the extrapolated measurements expressed in tons per 24 hours. Note that  
791 vertical scale for observed masses has been scaled by a factor 2.4 to be comparable with extrapolated masses. Light blue  
792 diamonds represent Mobile-DOAS average daily SO<sub>2</sub> measurements expressed in tons per 24 hours and green diamonds  
793 individual measurements. Observed masses, when multiplied by a factor of 2.4, are consistent during eruptive phases with  
794 the extrapolated DOAS and Mobile DOAS values.

795 **Figure 8.** Comparison between SO<sub>2</sub> *observed masses* (black bars) and SO<sub>2</sub> extrapolated masses (turquoise bars) during each  
796 eruptive phase since 2007. Daily observed masses are expressed in tons per ten hours and extrapolated masses are expressed  
797 in tons per 24 hours with separate vertical scales on the left of the plots. The vertical scale for the observed masses is 2.4  
798 times smaller so that curves are directly comparable. White background indicates periods of quiescence. Yellow and orange  
799 represent low (LEA) and high explosive activity (HEA) respectively. Cumulative SO<sub>2</sub> emission based on observed masses  
800 (in t/10h) is shown as a thick blue line. Time scale is indicated in number of days since January 1 for each year at the bottom  
801 of each diagram and calendar dates are indicated at the top. The different plots a) to l) correspond to the phases of activity  
802 described in Table 1 and the Supplementary Material. During the HEA and most of the LEA episodes SO<sub>2</sub> observed masses  
803 (multiplied by 2.4) are fairly the same as the SO<sub>2</sub> extrapolated masses. During quiescence SO<sub>2</sub> observed masses are much  
804 lower than the corresponding extrapolated mass. Red arrows indicate the days when long run-out pyroclastic flows were  
805 produced.

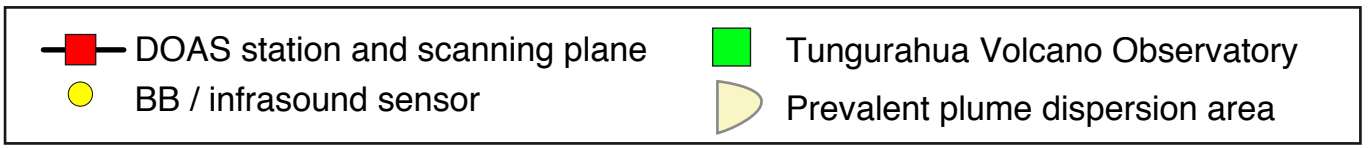
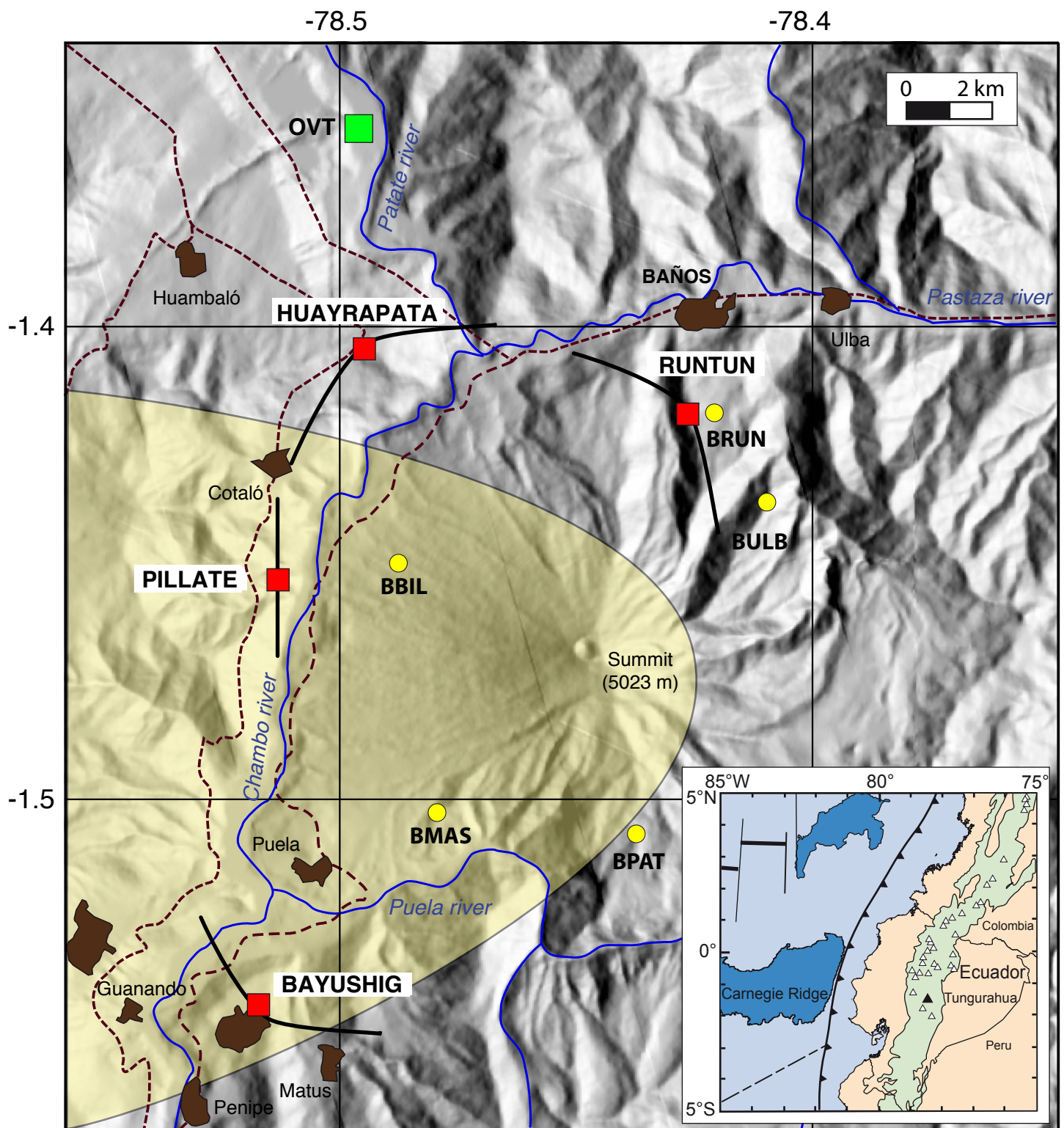
806 **Figure 9.** Total released observed mass of SO<sub>2</sub> multiplied by 2.4 for each phase of activity plotted as a function of phase  
807 duration. Results from the model presented in the Appendix and discussed in section 6.4 are given in the inserted box.

808

## 809 TABLE CAPTIONS

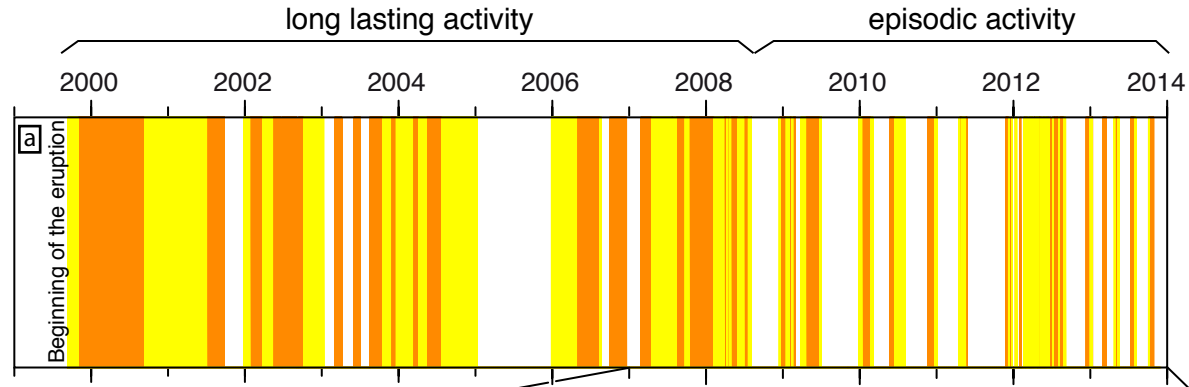
810 **Table 1** Summary of the main characteristics of each eruptive phase since February 2007. “Beginning of the phase” refers  
811 to the type of onset. Sudden awakening of the volcano is typically characterized by a strong Vulcanian eruption with  
812 intermediate to long run-out pyroclastic flows. Progressive refers to an *in crescendo* increase in the intensity of the activity,  
813 mainly Strombolian in style. To describe the eruptive sequences we use L for low explosive activity (LEA), H for high  
814 explosive activity (HEA). Average and maximum plume heights were obtained from the Washington VAAC  
815 (<http://www.ssd.noaa.gov/VAAC/messages.html>), which is constructed from visual or satellite observations. The  
816 average SO<sub>2</sub> emission and total cumulated SO<sub>2</sub> calculated using the *observed masses* method are shown (t/10h). For  
817 comparison with other volcanoes we also show total values multiplied by 2.4. Average SO<sub>2</sub> emissions during HEA and LEA  
818 episodes for each phase and quiescence are also shown.

819





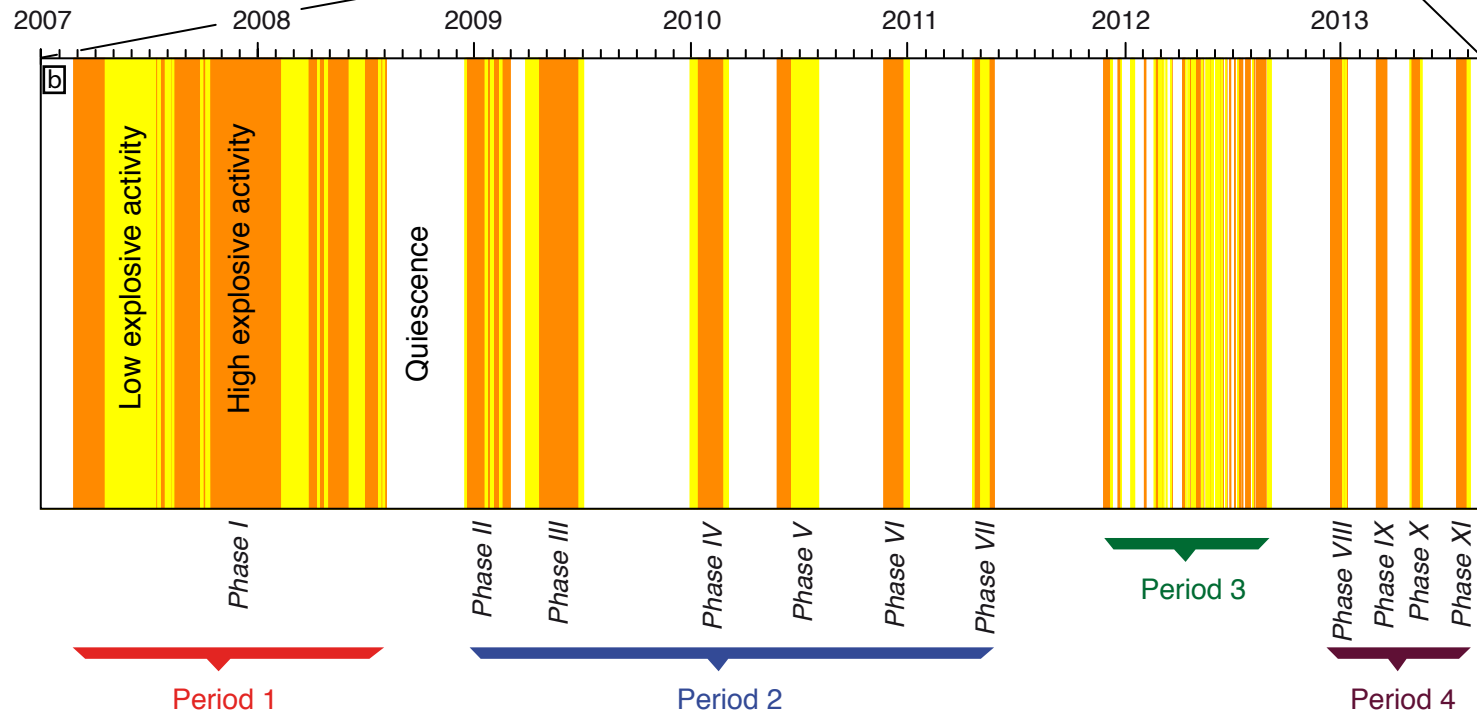
c



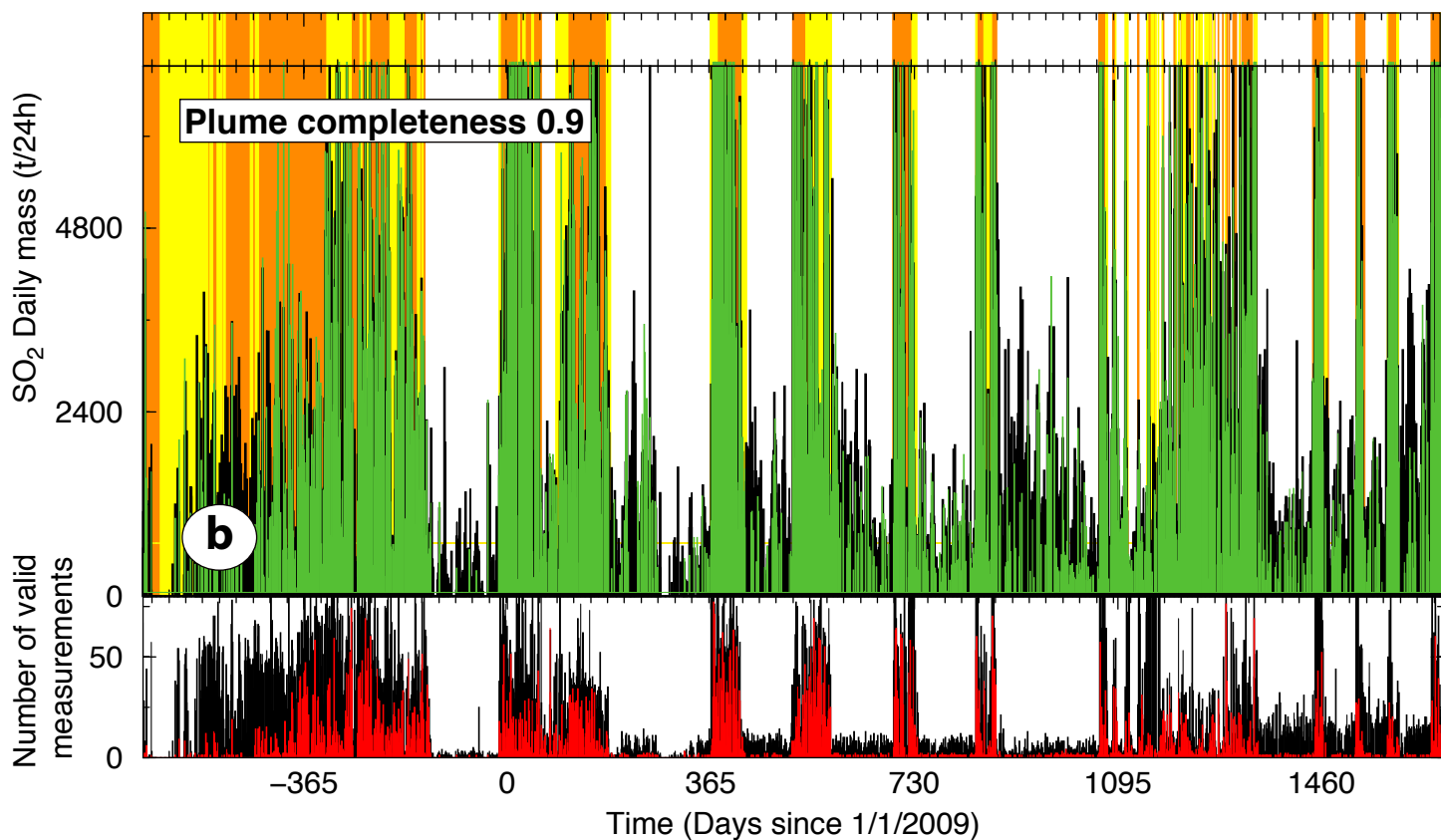
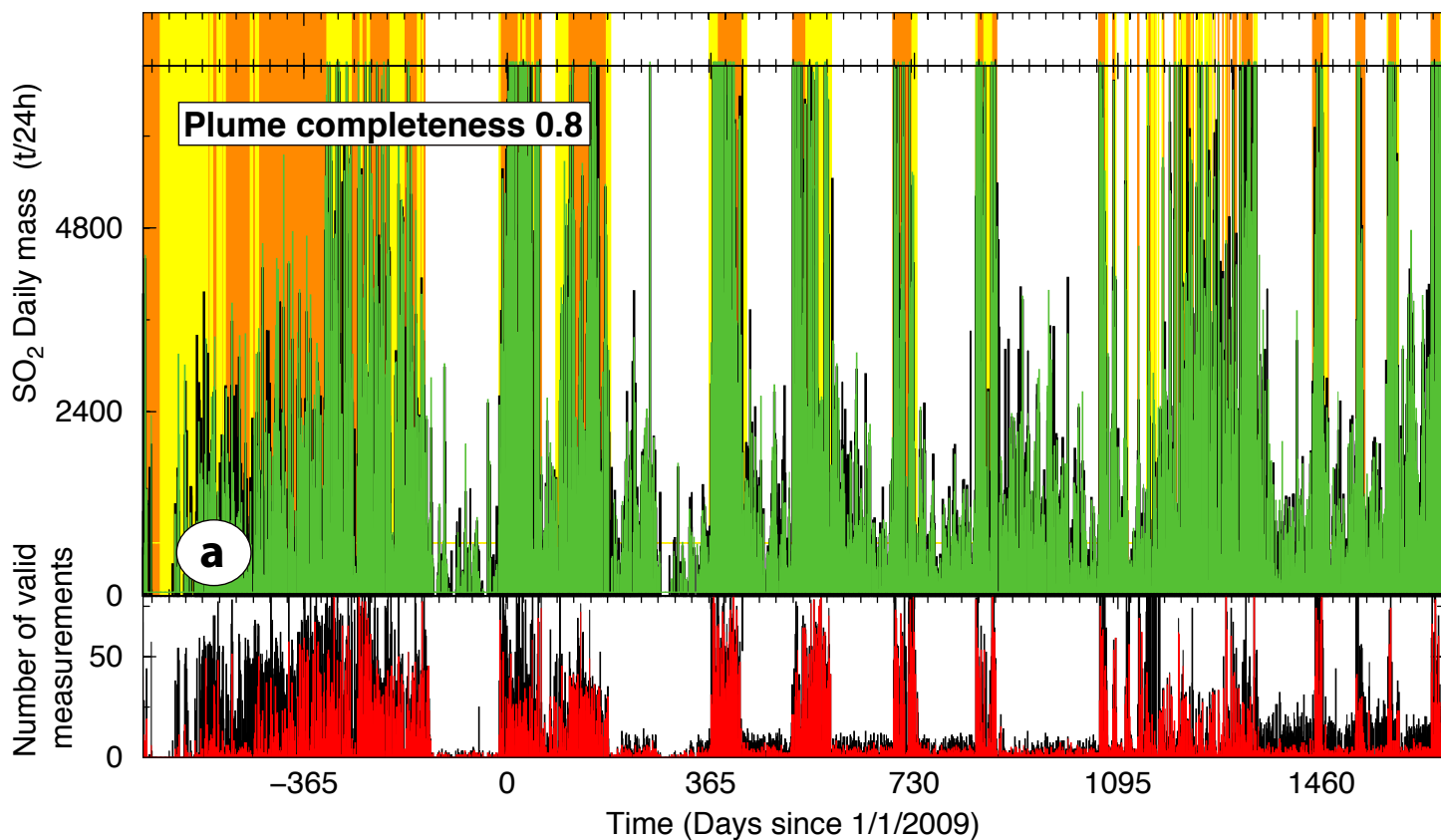
d

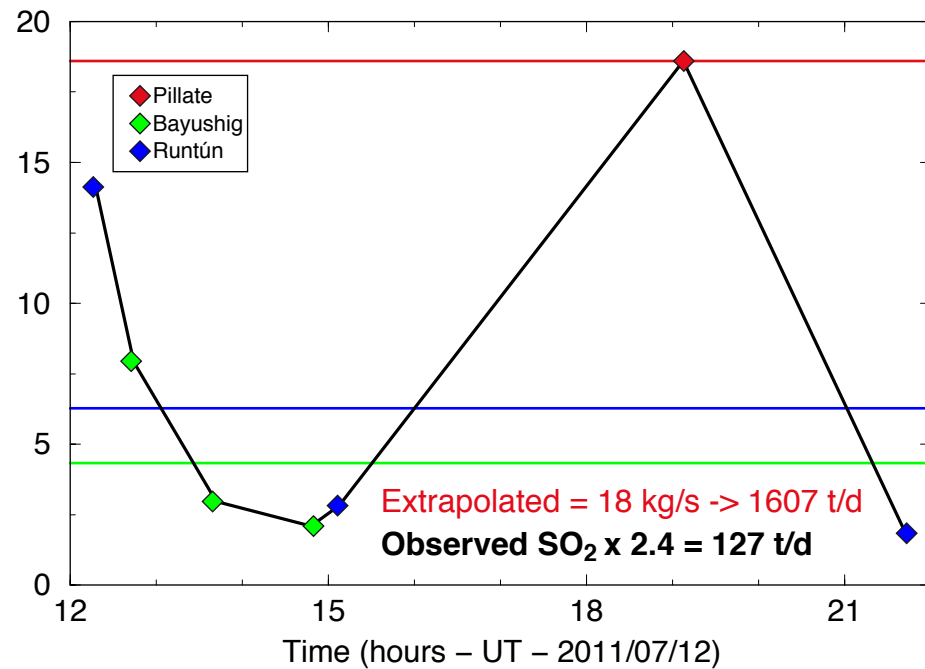
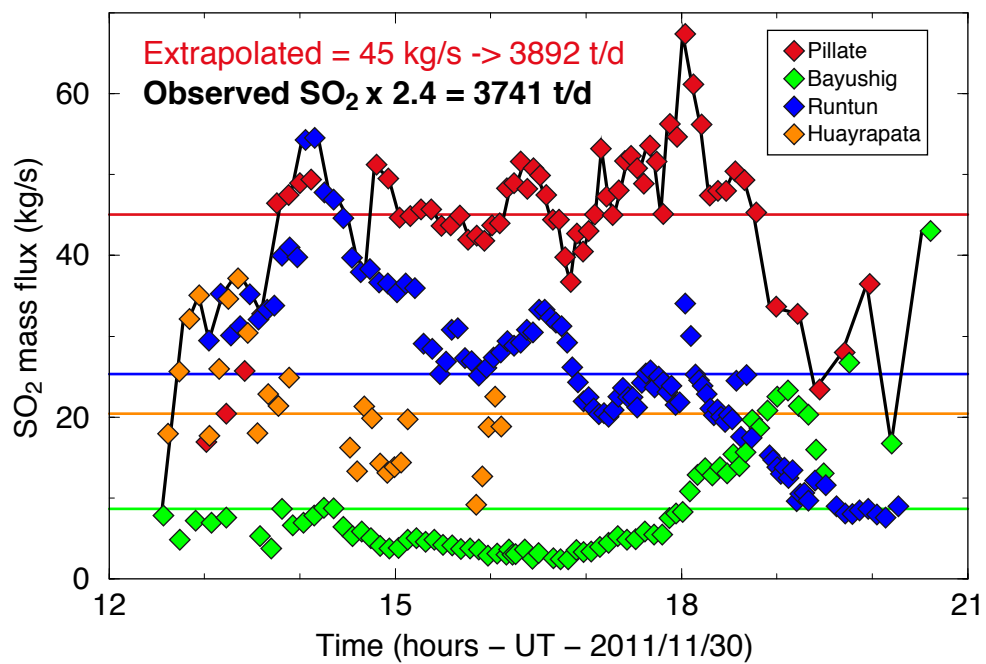


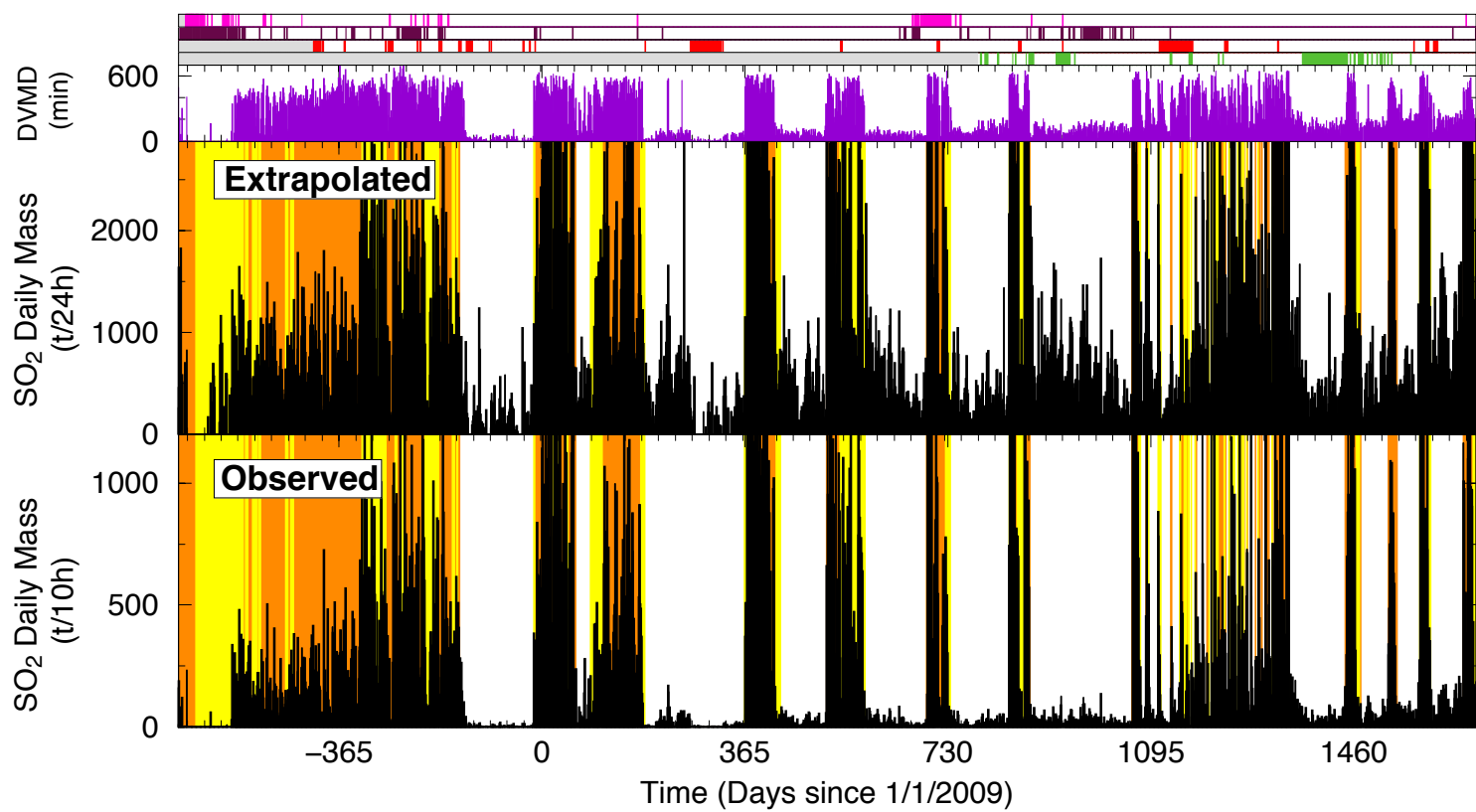
e

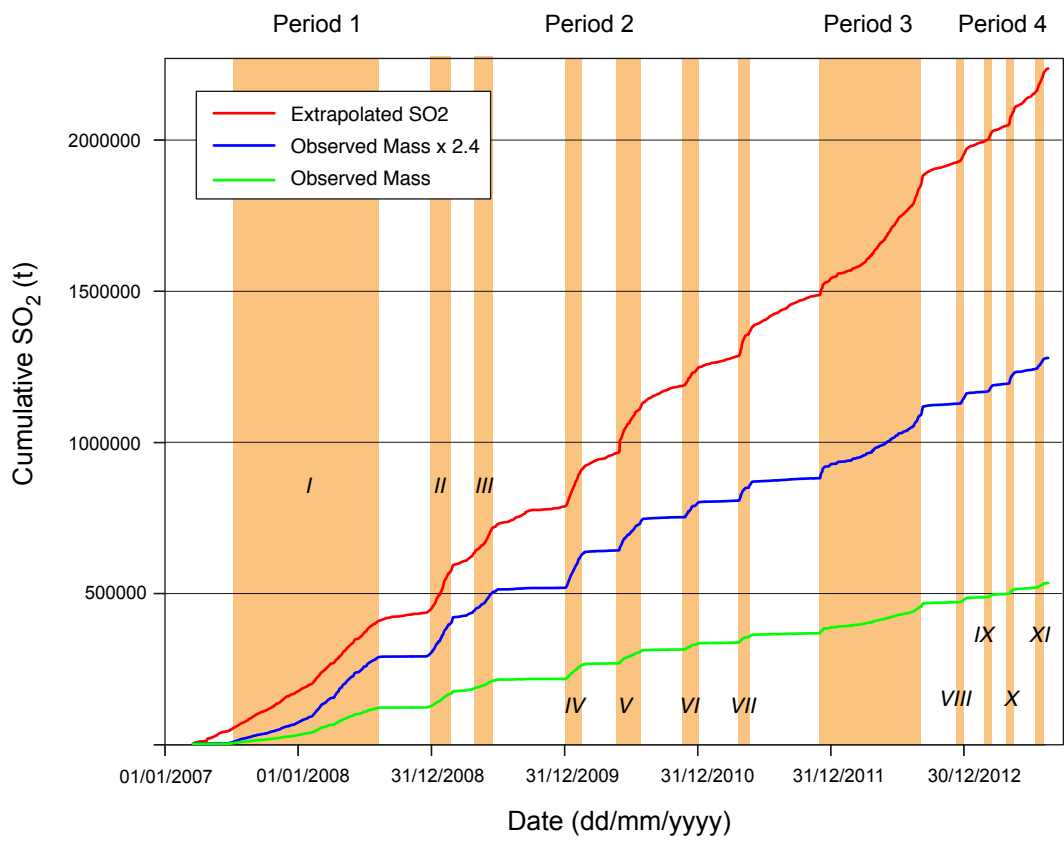


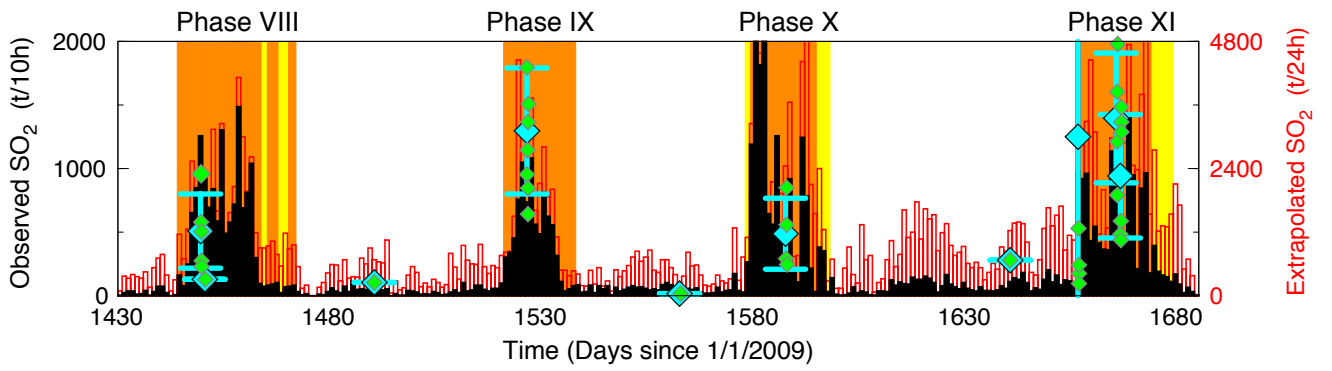
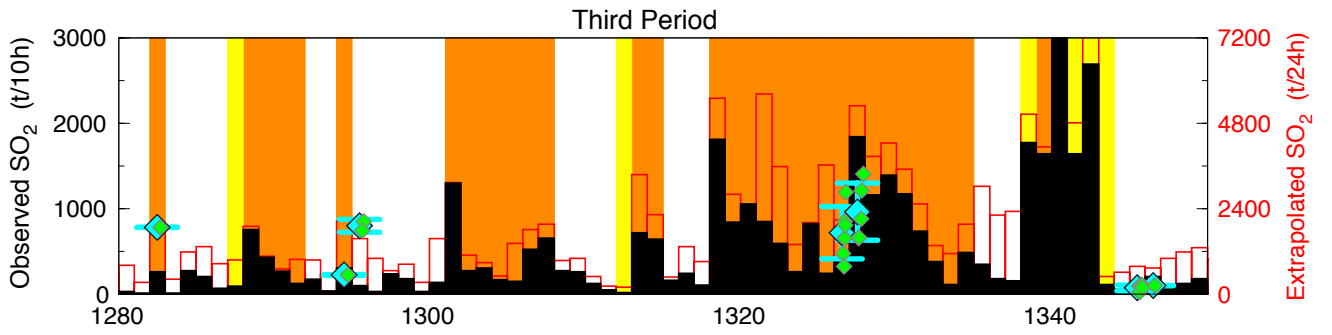
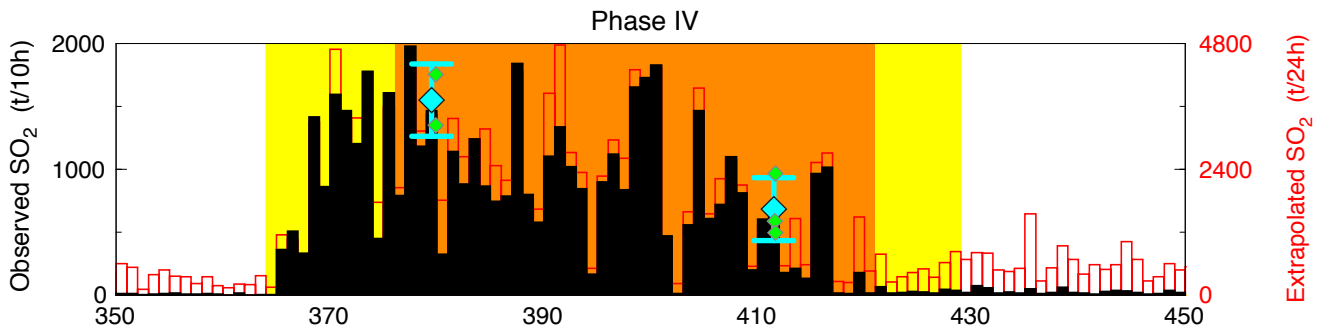
f

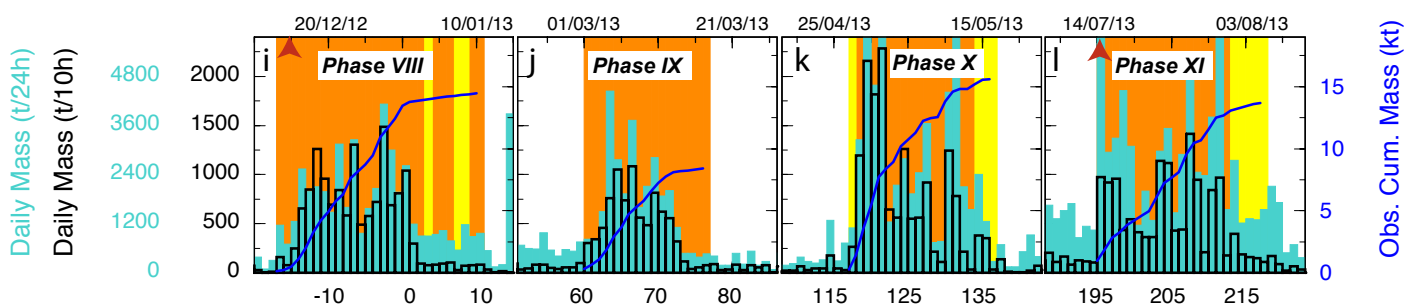
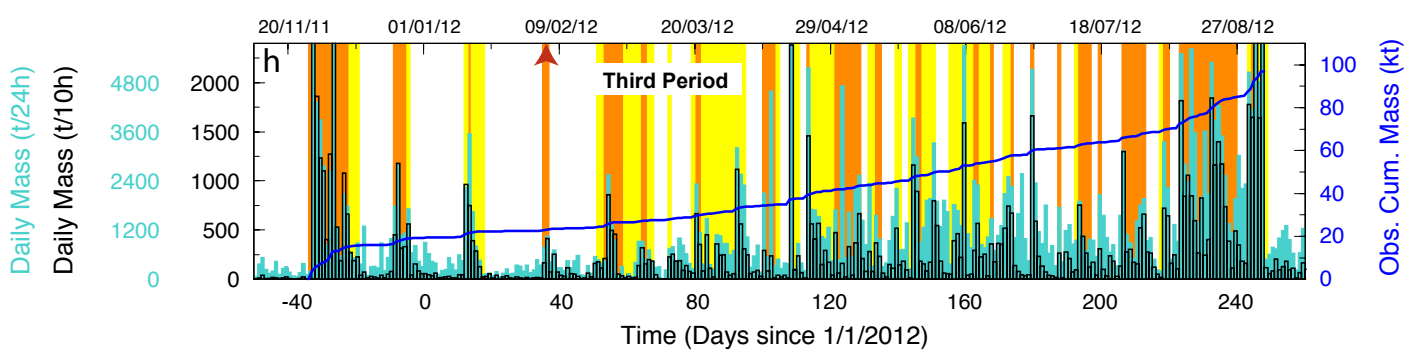
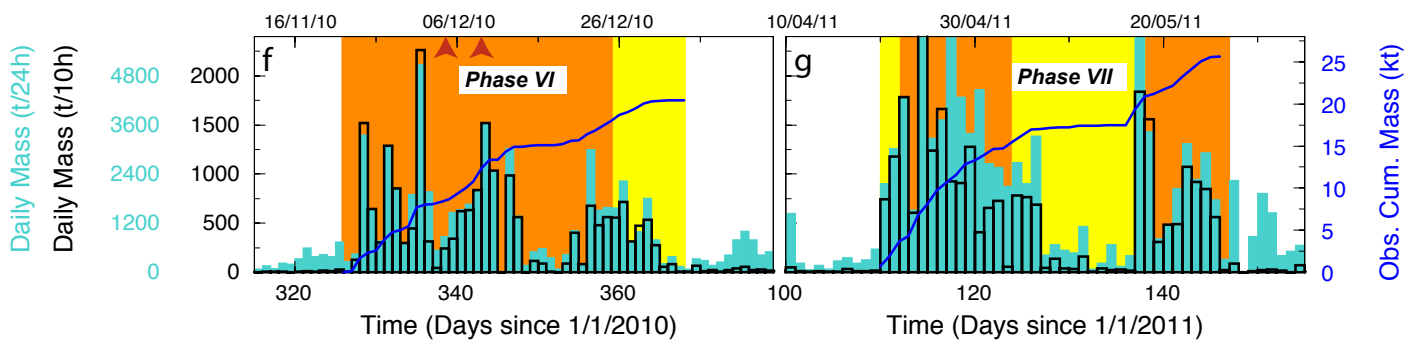
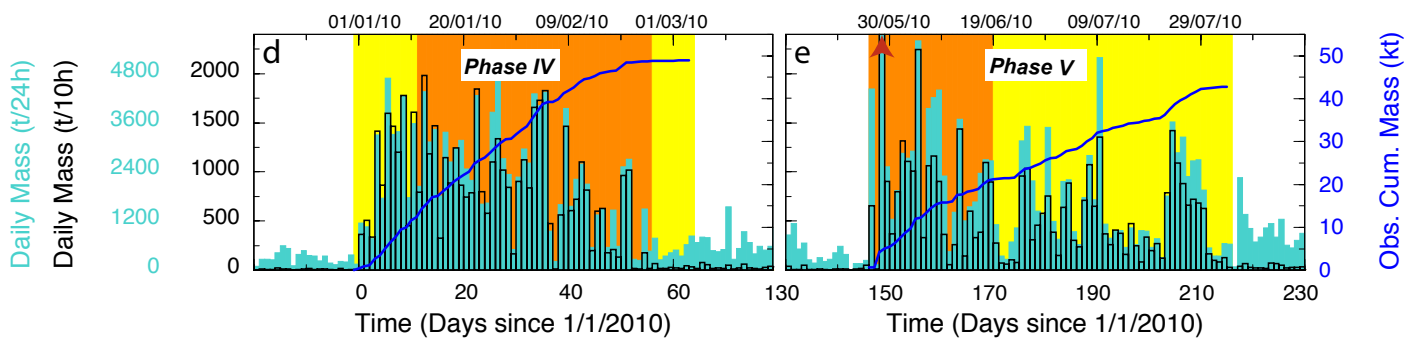
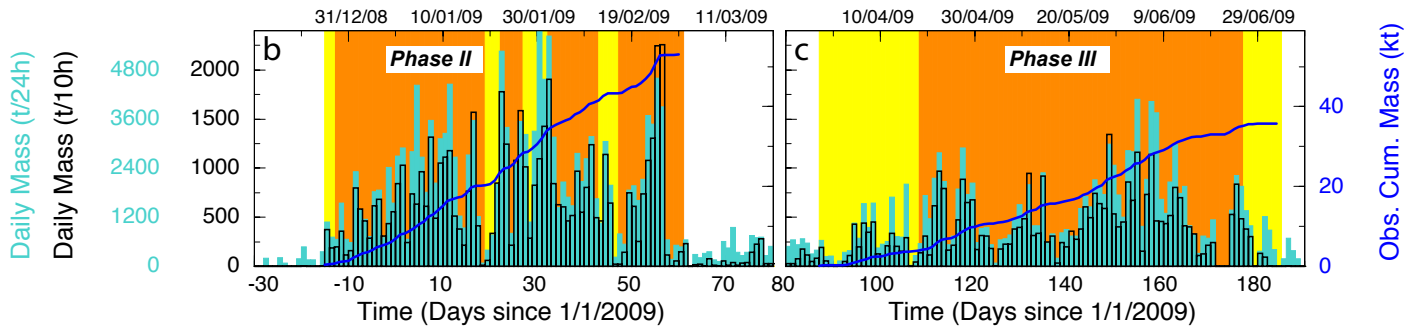
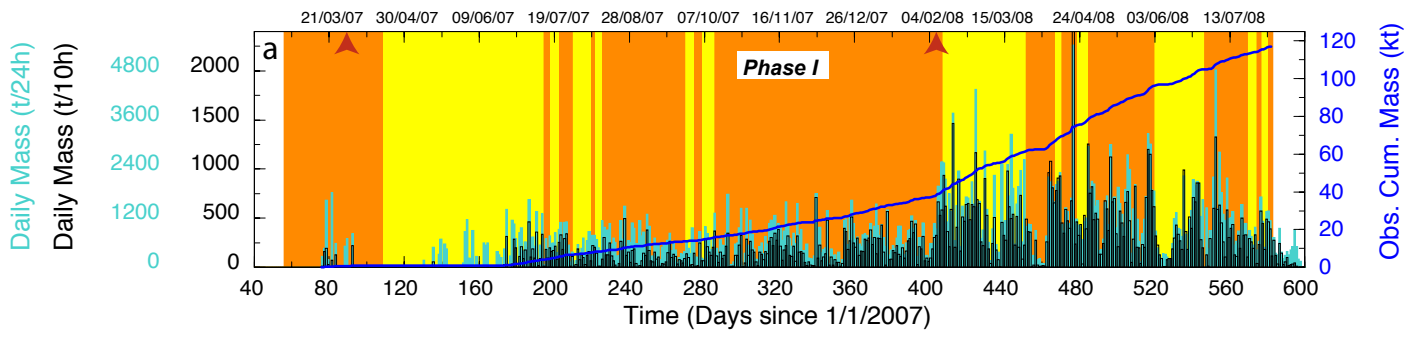


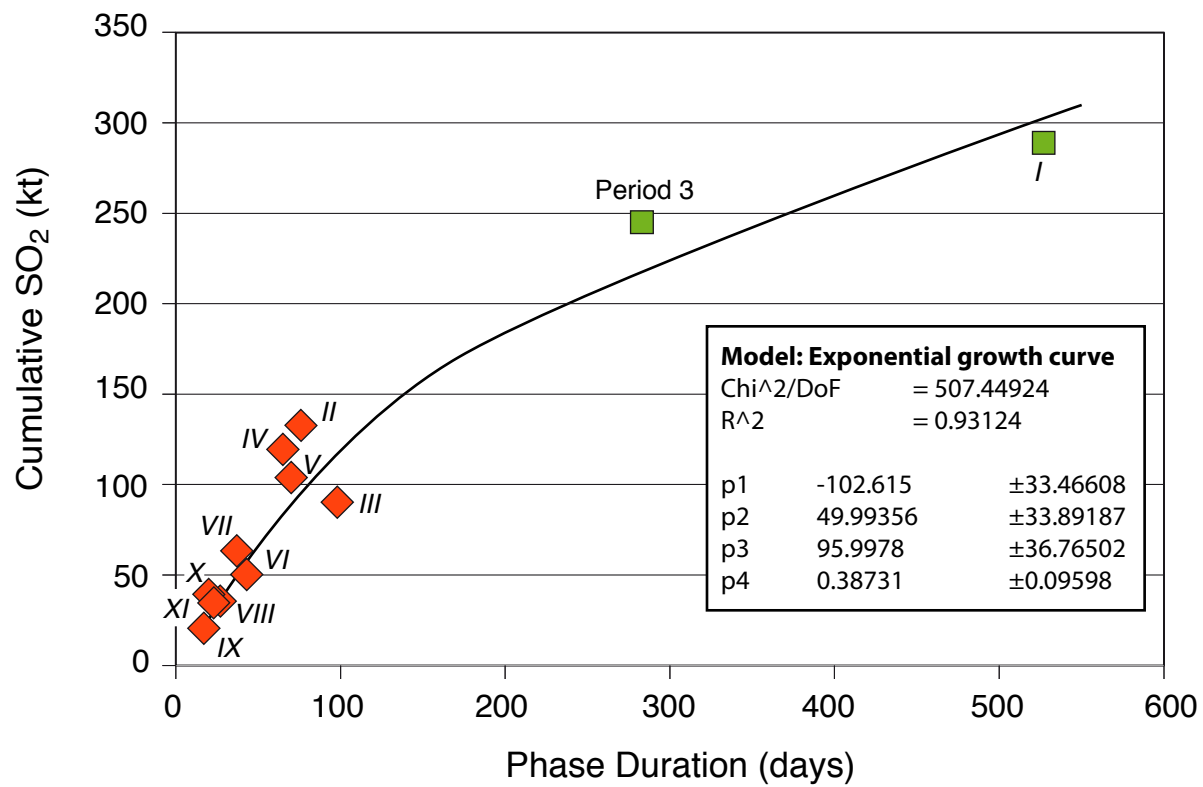


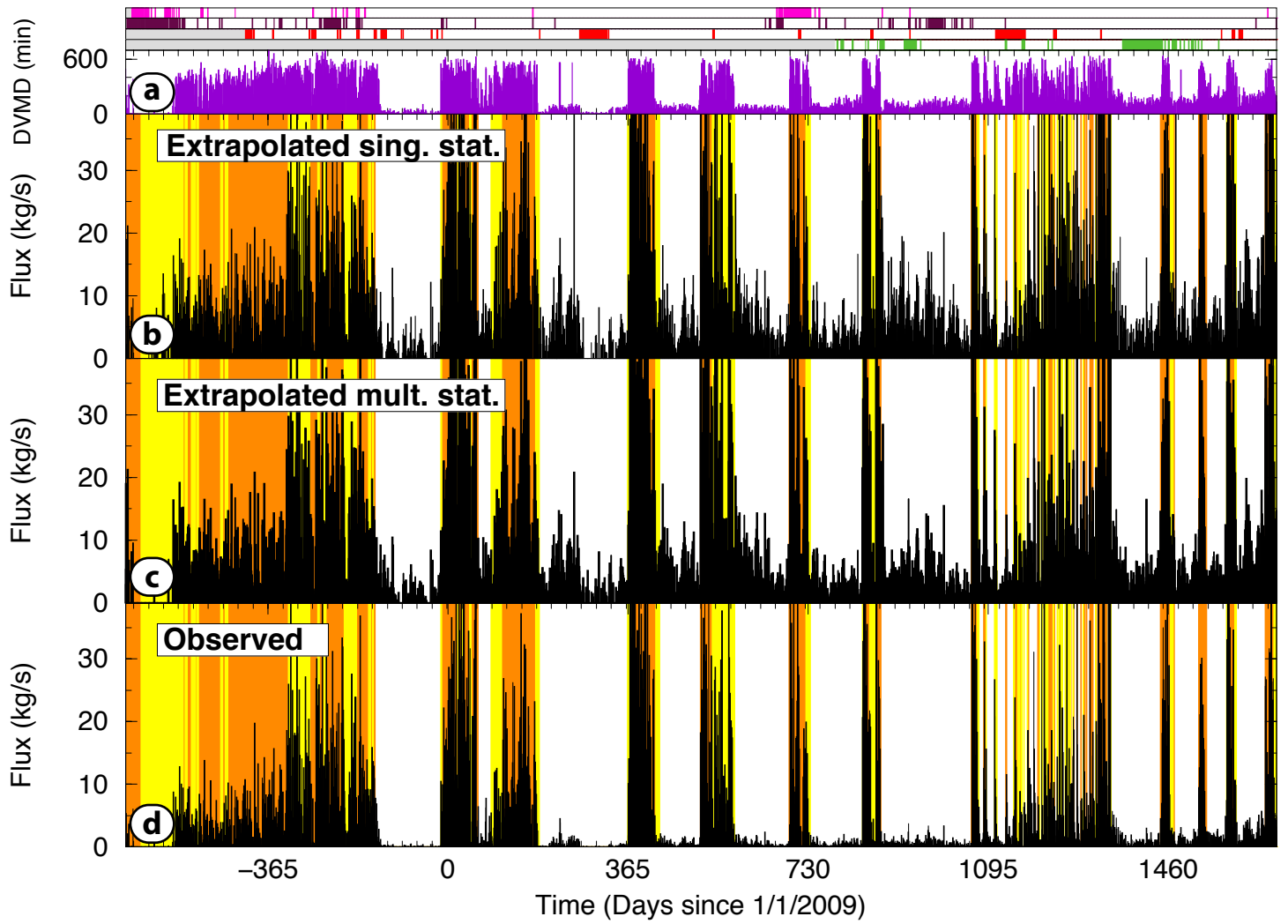












Extrapolated masses (traditional approach), shown in t/24h in the manuscript, can be expressed in kg/s by making the corresponding units conversion. This value represents the average SO<sub>2</sub> flux for the whole day independently of the duration of validated measurements (daily validated measurement duration or DVMD, Figure 1a). This value corresponds to the highest mean flux among all stations and can be seen as a Single Station extrapolated flux (Figure 1b).

When using the observed masses which are an integration of the highest fluxes among all stations, and dividing the result by the DVMD we obtain time series very similar to the extrapolated masses (traditional approach) with the difference that we use the four stations for the calculation instead of the higher average among them. This could be considered as a multi-station extrapolation (Figure 1c).

An observed flux expressed in kg/s can be obtained by dividing the observed masses by the observation time, which is 10 hours at Tungurahua, as stations actually work for that period of time independently of the activity of the volcano. This observed flux is equivalent to the observed masses except for the units in which it is expressed (Figure 1d).

As seen in Figure 1 all these 3 different approaches are fairly equivalent during activity phases, when DVMD is around 600 minutes. During quiescent phases only the observed fluxes reflects well the actual absence of volcanic activity with a corresponding low SO<sub>2</sub> degassing.

Figure caption

Figure 1. SO<sub>2</sub> fluxes (kg/s) time series for Tungurahua volcano between 2007 and 2013. a. Daily validated measurement duration. b. Extrapolated fluxes calculated by using the higher average among 4 stations. c. Extrapolated fluxes calculated by dividing the total integrated SO<sub>2</sub> among 4 stations for the DVMD. d. Observed fluxes calculated by dividing the total integrated SO<sub>2</sub> among 4 stations by the observation time (10 hours at Tungurahua).

## Supplementary Material

### Detailed description of the eruptive phases of Tungurahua since 2007 until August 2013

#### *First Period (527 days)*

##### *Phase I: 24-02-2007 to 04-08-2008 (repose 68 days, duration 527 days)*

This 527-day phase is characterized by 13 episodes of HEA lasting from 2 to 123 consecutive days, alternated with LEA (Figure 8a). Two pyroclastic flows, extending 1 and 5 km from the vent, were produced on March 27, 2007 (86) and February 6, 2008 (401) respectively. DOAS stations worked properly from June 22, 2007 (172). SO<sub>2</sub> daily observed masses were almost constant around 300 t/10h until February 8, 2008 (403), two days after the second episode producing pyroclastic flows. Since then the average *observed* mass almost doubled presenting variations not necessarily according to the type of activity (HEA or LEA). Indeed between February 11 (406) and March 25 (450) no significant explosions were recorded, but SO<sub>2</sub> emissions were higher than during precedent HEA episodes of this phase.

#### *Second Period (892 days)*

##### *Phase II: 16-12-2008 to 01-03-2009 (repose 132 days, duration 76 days)*

In this phase we find HEA interspersed with four short-lasting (up to 4 days) LEA episodes (Figure 8b). SO<sub>2</sub> observed mass shows a progressive increase up to 1800 t/10h. These values then progressively decrease until the end of the phase, with, however, a degassing peak before the end of the episode (2250 t/10h). The cumulative SO<sub>2</sub> emission shows a constant slope but reaches a plateau in the last 5 days of activity.

##### *Phase III: 28-03-2009 to 03-07-2009 (repose 26 days, duration 98 days)*

This phase is composed by LEA episodes at the beginning and end, enclosing a HEA episode (Figure 8c). The first LEA episode took place from March 28 (87) until April 17 (107). SO<sub>2</sub> emission was below 500 t/10h before the high-energy explosions started on April 18 (108). During the HEA the SO<sub>2</sub> emission was variable, fluctuating between 100 t/10h and 1300 t/10h. The closing LEA episode lasted 8 days between June 26 until July 3 (184) showing a rapid decrease in SO<sub>2</sub> emission since the end of the HEA. SO<sub>2</sub> was measured until June 29, while some ash and gas emissions were still produced until July 3. The slope of the SO<sub>2</sub> cumulative emission curve is variable with fluctuations due to several peaks of degassing.

##### *Phase IV: 30-12-2009 to 04-03-2010 (repose 179 days, duration 65 days)*

Similarly to the previous phase LEA preceded and followed the main HEA episode, which lasted from January 11 (11) to February 24 (55) (Figure 8d). During the first LEA episode the activity progressively increased in intensity. SO<sub>2</sub> degassing stepped-up from non-detectable to more than 1700 t/10h during the first 11 days of LEA. During the following HEA episode the SO<sub>2</sub> emission values were variable with a global decrease since February 6 (36). Ash emissions continued until March 4 (63) but no significant SO<sub>2</sub> was measured during the last days of activity (Figure 8d).

*Phase V: 26-05-2010 to 03-08-2010 (repose 82 days, duration 70 days)*

Activity began with a phreatic explosion on May 26. This phase is composed of an episode of HEA, which started the phase, followed by a LEA episode (146, Figure 8e). No gas or ash emissions preceded this event, which was also characterized by the absence of precursory signs such as an increase of seismicity or changes in the tilt-meter records (OVT weekly reports). A first peak of SO<sub>2</sub> emission was related to the phreatic explosion (660 t/10h). Little seismicity and no degassing were observed on May 27. On May 28 (148) a Vulcanian explosion produced an 8.8 km high eruptive column blowing out blocks, gas and ash. Besides, several intermediate run-out pyroclastic flows (4.5 from the vent) were produced associated with this explosion. These observations suggest that the volcano was in a state of closed system, blocked by a lava plug, which was partially blown by the explosion of May 26 and then almost completely removed with the Vulcanian explosion of May 28. After this, HEA continued until June 18 (169) and LEA with ash and gas emissions persisted until August 3 (215). SO<sub>2</sub> emissions were variable but persistent during the whole phase, being higher during the HEA episode, in particular on May 28 and June 4 (~ 2200 t/10h). Low SO<sub>2</sub> emissions were observed just after the HEA episode and between July 10 and 22 (191-203; ~ 300 t/10h). Several changes in slope are observed in the cumulative curve, with the major slope corresponding to the first 18 days of HEA.

*Phase VI: 22-11-2010 to 03-01-2011 (repose 110 days, duration 43 days)*

This phase also begins with HEA, but the activity shows a progressive increment. A few days of LEA closed this phase (Figure 8f). Three episodes of SO<sub>2</sub> degassing roughly correlated with the occurrence of high-energy explosions can be distinguished: from November 22 to December 2 (326-336), December 4 to 13 (338-347) and December 19 to 31 (353-365). The activity started in the afternoon of November 22 with continuous ash venting and a few explosions. The first explosions of this phase occurred at 17:00 (local time) on November 22, so the SO<sub>2</sub> related to this activity could not be measured. SO<sub>2</sub> was detected since the second day of activity, but reached high values (>1500 t/10h) only on the third. Activity progressively increased the following days with a few high-energy and dozens of small explosions. The explosions lasted until December 25 (359) but a decrease in number was observed since December 13 (347). The maximum peak of SO<sub>2</sub> emission was detected on December 1 (335) reaching 2250 t/10h. SO<sub>2</sub> decreased rapidly on December 3 (337), one day before pyroclastic flows reaching 4 km from the vent were produced. Besides a lava flow reaching about 1.5 km from the vent descended on the night from December 4 to 5. A progressive increase in degassing is observed reaching a high value around 1500 t/10h on December 9 (343), when a single explosion produced a pyroclastic flow extending 3 km from the vent. After December 26 (360), ash and gas emissions were less continuous and reached progressively lower altitudes. Eruptive activity completely ceased on January 3 (3). The last episode of degassing (353-365) was accompanied by high-energy explosions only during the first six days. A variable slope in the SO<sub>2</sub> cumulative curve is observed with four decreasing slopes and a deceleration of the emission trend five days before the end of the eruptive activity.

*Phase VII: 20-04-2011 to 26-05-2011 (repose 106 days, duration 37 days)*

This phase is composed by two HEA episodes from April 22 (112) to May 3 (123) and from May 18 to 26 (138 to 146), each preceded by LEA (Figure 8g). Before both explosive episodes the opening of the conduit was relatively rapid (few hours) but progressive, characterized by sub-continuous ash venting. SO<sub>2</sub> values increased two days before the first HEA episode reaching between 740 and 1200 t/10h, and one day before the second HEA (1850 t/10h). Both increases occurred during LEA episodes in which strong ash venting was observed. Except for this last high emission value, SO<sub>2</sub> emission values were low (maximum 785 t/10h) during the LEA from May 4 to 17. In the first HEA episode, the SO<sub>2</sub> emission followed a bell-shape distribution with a peak on April 24 (2600 t/10h) and a progressive decrease until three days following the last explosion. During the second HEA episode two peaks of degassing are observed, at the beginning and in the middle of the episode (May 23-25). During the first HEA episode the SO<sub>2</sub> cumulative curve displays a progressively decreasing positive slope with a rapid stabilization during the LEA. Two different slopes are observed for the second episode (Figure 8g).

*Third Period (repose 184 days, duration 283 days)*

Several short-lived phases of activity were observed during this period. SO<sub>2</sub> emission is variable, being higher for the first and the last phases, which are also the longest of the period with 15 and 25 days respectively. These two phases are briefly described below, but they are not considered independently in this study but as a continuum within the third period. The SO<sub>2</sub> cumulative emission curve shows several steps corresponding mainly to the HEA episodes (Figure 8h).

*27-11-2011 to 11-12-2011 (duration 15 days)*

The activity followed a 184-day period of quiescence (Figure 8h). It is composed of a HEA episode followed by a few days of LEA. Intense fumarolic activity was observed on November 26 (-35) on the northeastern flank of the volcano and three VT earthquakes were recorded on the 27 (-34). High-energy explosions then occurred, lasting until December 8 (-23). Two peaks in degassing around 3400 t/10h were measured on November 28 and December 4, associated with intense surface activity and the presence of a higher number of explosions. SO<sub>2</sub> was no longer detected after December 10 (-21), two days after the end of the HEA, but small ash emissions were observed until December 11 (-20).

*22-12-2011 to 06-08-2012 (repose 10 days, duration 228 days)*

During this period the volcano remained as an open system with continuous gas and ash venting activity and sporadic explosions. Several very short periods of quiescence lasting less than 17 days and more typically around 4 days were observed. One 3 km-long pyroclastic flow was produced on February 4. SO<sub>2</sub> values are variable showing some peaks associated indistinctly with HEA or LEA (Figure 8h) on April 1 (1220 t/10h), 17 (2500 t/10h), 22 (1500 t/10h), May 23 (1200 t/10h), June 7 (1650 t/10h) and 27 (1900 t/10h). Looking at the cumulative curve for the whole period between December 22, 2011 (-9) and August 6, 2012 (219) we note a progressive increase of the slope indicating an increasing SO<sub>2</sub> degassing until the occurrence of the last episode within this period.

*10-08-2012 to 04-09-2012 (duration 25 days)*

After 3 days of quiescence strong eruptive activity resumed with an explosion whose ash column reached 2 km above the crater. Seismic tremor had high amplitude in this phase during which continuous ash emissions was observed. The activity peaked on August 18 (230) with a continuous emission resulting in a 4-km-high ash column. SO<sub>2</sub> degassing was observed during the whole HEA until August 26 (238). Two peaks of degassing at more than 1500 t/10h occurred at the beginning of the phase and on August 19 (231) each was characterized by a rapid increase followed by a progressive decay. Three days without surface activity followed this episode (27-29 August) but emission activity then resumed until September 4 (247). SO<sub>2</sub> emission was high during these last days, reaching 4500 t/10h on September 1 (243).

*Fourth Period (235 days)*

*Phase VIII: 14-12-2012 to 10-01-2013 (repose 101 days, duration 27 days)*

On December 14 (-17) at 19:36 UTC, a Vulcanian explosion initiated the phase, with an associated ash column reaching 7 km above the crater. After this explosion the activity slowed down for less than one day with only a few small explosions, fumaroles and the generation of a small reddish ash column. The volcano renewed its activity on December 16 (-15) at 8:20 UT with a sustained and violent Strombolian activity which persisted with a decreasing intensity until January 1 (1). Seismicity was particularly high during 4 days starting on December 16 (-15) with high amplitude tremor and explosion quakes. On December 16 (-15), Vulcanian activity was observed and produced pyroclastic flows that reached a distance of about 3.5 km from the crater. Significant explosions were recorded until December 29 (-2), but since the 21 their number and energy diminished. A few small explosions were recorded on January 4-6 (4-6) and 9-10 (9-10) with few days of LEA in between. The measured SO<sub>2</sub> emission during the first 3 days of this phase was relatively low (< 300 t/10h) and then increased progressively to reach 1300 t/10h on December 19 and 24. SO<sub>2</sub> fluxes remained around 1000 t/10h until December 31 when degassing dropped to a low level for the remaining part of the phase, coincident with the disappearance of significant explosions. A single slope is observed in the cumulative SO<sub>2</sub> curve with a clear leveling out at the end of the phase (Figure 8i).

*Phase IX: 01-03-2013 to 17-03-2013 (repose 49 days, duration 17 days)*

Only HEA was observed during this phase. Activity increased progressively with sporadic explosions and permanent ash and gas emissions. The activity was typically Strombolian with some Vulcanian explosions. The magma flux sustaining the Strombolian activity seemed almost constant until March 13 (72) when the number of explosions increased and produced higher ash columns reaching up to 3.3 km above the crater. On March 16 (75) there was a small peak in the activity with 4 consecutive Vulcanian explosions. After this episode the activity rapidly decreased and ended on March 17, when only water vapor emission was observed. SO<sub>2</sub> was detected since the onset of explosive activity and increased gradually to reach values between 750 and 1100 (t/10h) between March 4 and 7 (63-66). After this, it progressively decreased to non-detectable levels on March 14 (73). SO<sub>2</sub> flux values for this phase show a

bell-shaped distribution (Figure 8j). A constant slope is observed in the cumulative SO<sub>2</sub> curve with a clear flattening at the end of the phase.

*Phase X: 27-04-2013 to 16-05-2013 (repose 41 days, duration 20 days)*

One day of LEA started this phase, with a slight increase in SO<sub>2</sub> emission up to 275 t/10h. On April 28, HEA began with the SO<sub>2</sub> flux rapidly increasing up to 2250 t/10h during the second (April 29, 119) and fourth (May 1, 121) days of explosive activity. A new peak in SO<sub>2</sub> emission was observed three days before the end of the HEA phase on May 10 (130). The emission of SO<sub>2</sub> decreased rapidly during the closing LEA episode (Figure 8k). Ash emission was continuous during this phase but columns were typically low, reaching on average 2 km above the crater. This phase has the highest SO<sub>2</sub> daily average emission of the entire fourth period, probably related to the continuous surface activity.

*Phase XI: 14-07-2013 to 05-08-2013 (repose 58 days, duration 23 days)*

The eruptive phase started on July 14 (194) with a Vulcanian explosion, which produced an ash, blocks, and gas eruption column that ascended up to 9 km above the crater. This sudden opening of the volcanic conduit produced long run-out pyroclastic flows, which reached the Chambo river (6.5 km from the vent) through several ravines, making this event similar to those produced on July 14, 2006 (Samaniego et al. 2011) and May 28, 2010. This major event was only preceded by an increase in LP seismicity starting on July 12 (192). The Vulcanian explosion was followed by several hours of volcanic tremor while vapor columns with low ash content were observed at the surface. A significant drop in activity was observed on July 15 but strong explosive activity renewed on July 16 (196) progressively escalating in number until July 21 (201). A new peak in explosive activity was recorded on July 28 (208). Sub-continuous tremor with interspersed explosions lasted until July 31 (211). SO<sub>2</sub> globally followed the explosive activity, showing four peaks around 1000-1500 t/10h (Figure 8l). After the end of the HEA the emission activity continued until August 5 (216) with low values of SO<sub>2</sub> emission (100-400 t/10h).